https://doi.org/10.5194/essd-2026-418
Preprint. Discussion started: 24 July 2026

Open Access Earth System Science Data Discussions

Improved estimation of net ecosystem CO_2 exchange over North America using LSTM-based flux upscaling (2001–2021)

Chengcheng Huang[1], Wei He[2,3], Brendan Byrne[4], Ngoc Tu Nguyen[5], Jingfeng Xiao[6], Hua Yang[7], Phillipe Ciais[8], Songhan Wang[9], Xing Li[10], Han Ma[11,12], Peipei Xu[13], Mengyao Zhao[13], Hui Chen[10], Weimin Ju[3]

[1]State Key Laboratory of Earth Surface Processes and Disaster Risk Reduction, Faculty of Geographical Science, Beijing Normal University, Beijing 100875, China
[2]Zhejiang Carbon Neutral Innovation Institute & Zhejiang International Cooperation Base for Science and Technology on Carbon Emission Reduction and Monitoring, Zhejiang University of Technology, Hangzhou, Zhejiang 310014, China
[3]International Institute for Earth System Science, Nanjing University, Nanjing, Jiangsu 210023, China
[4]Jet Propulsion Laboratory, California Institute of Technology, Pasadena, CA, USA
[5]State Key Laboratory of Hydrology-Water Resources and Hydraulic Engineering, College of Hydrology and Water Resources, Hohai University, Nanjing, Jiangsu 210024, China
[6]Earth Systems Research Center, Institute for the Study of Earth, Oceans, and Space, University of New Hampshire, Durham, NH, USA
[7]State Key Laboratory of Remote Sensing and Digital Earth, Faculty of Geophysical Science, Beijing Normal University, Beijing 100875, China
[8]Laboratoire des Sciences du Climat et de l'Environnement, LSCE/IPSL, CEA-CNRS-UVSQ, Université Paris-Saclay, Gif-sur-Yvette, France
[9]Jiangsu Collaborative Innovation Center for Modern Crop Production, Key Laboratory of Crop Physiology and Ecology in Southern China, Nanjing Agricultural University, Nanjing, China
[10]School of Geography and Planning, Sun Yat-sen University, Guangzhou, China
[11]JC STEM Lab of Quantitative Remote Sensing, Department of Geography, The University of Hong Kong, Hong Kong, China
[12]International Center for China Development Studies, The University of Hong Kong, Hong Kong, China
[13]School of Geography and Tourism, Anhui Normal University, Wuhu, Anhui 241002, China

Correspondence to: Wei He (wei.he@zjut.edu.cn)

Abstract. Accurate estimation of regional-scale terrestrial carbon budgets is of great importance but remains challenging. With particular advantages, the Long Short-Term Memory (LSTM) networks method shows potential in improving regional carbon budget upscaling estimations. Here, based on LSTM, we upscale regional net ecosystem carbon exchange (NEE) with available flux tower measurements and satellite land surface observations in North America. With well-established ecosystem-specific LSTMs, we produced monthly NEE at a spatial resolution of 0.1° × 0.1° over 2001–2021 (labelled as MemoryFlux). Unlike existing upscaling estimates, our dataset properly identified the Midwest Corn Belt as a region of large seasonal carbon uptake during peak growing seasons, a feature revealed by previous top-down studies and recognized as a model benchmark. Moreover, the estimated seasonal variations of NEE by MemoryFlux coincided well with those by atmospheric inversions, i.e., the ensemble mean of Orbiting Carbon Observatory-2 Model Intercomparison Project (OCO-2 v10 MIP; $r = 0.96$, $p < 0.001$) and CarbonTracker2022 (CT2022) ($r = 0.97$, $p < 0.001$). The mean annual NEE was estimated at -1.27 ± 0.12 Pg C yr^{-1}, aligning more closely with the inversions (-0.83 to -0.70 Pg C yr^{-1}) than existing upscaling estimates (-3.30 to -1.68 Pg C yr^{-1}) do. In addition, our estimate plausibly captured the NEE spatial anomalies caused by all the recent extreme drought and flood events. We further confirmed that considering memory effects was critical for better indicating interannual variability and spatial anomalies of NEE induced by climate extremes. MemoryFlux provides an improved bottom-up estimation of North American NEE, largely narrowing the gap with top-down inversions. This dataset can be downloaded at https://doi.org/10.5281/zenodo.20482274 (Huang and He, 2026).

Keywords: Net ecosystem CO_2 exchange, Carbon flux upscaling, Interannual variations, Memory effect, Long Short-Term Memory (LSTM) networks

1 Introduction

Terrestrial ecosystems, as an important carbon sink on the Earth, absorb approximately one fourth of the carbon dioxide (CO_2) released by human activities, which significantly slows down the rising CO_2 in the atmosphere and the pace of global warming (Friedlingstein et al., 2022). Net ecosystem CO_2 exchange (NEE), defined as the difference between the CO_2 released by total ecosystem respiration and the CO_2 sequestered by photosynthesis (Ballantyne et al., 2021), indicates the current net carbon balance of terrestrial ecosystems. Climate extremes, e.g., droughts, floods, heatwaves, and wildfires, strongly impact terrestrial CO_2 exchange processes, leading to non-negligible interannual variations (IAVs) in the ecosystem carbon budget (Le Quéré et al., 2018). Accurate quantification of NEE at regional and global scales is essential for advancing our understanding of carbon-climate feedbacks (Yao et al., 2018).

NEE is only measurable at the plot scale with the eddy covariance (EC) technique (Wofsy et al., 1993), and cannot be observed directly over large scales. Feasible ways to estimate large-scale NEE include top-down inversion of atmospheric CO_2 concentration measurements and bottom-up estimation using process-based terrestrial biosphere models (TBMs) and data-driven machine learning upscaling. In recent years, the availability of atmospheric CO_2 observations has been greatly enhanced by space-based observations (Byrne et al., 2019), making it possible to infer the large-scale space-time distribution of carbon fluxes by using transport models and atmospheric CO_2 data. Compared to the bottom-up estimates, top-down inversions based on atmospheric CO_2 data provide a seasonal cycle of NEE that is more consistent with atmospheric CO_2 observations by assimilating the loss of CO_2 from various carbon release and transport pathways (Byrne et al., 2018). However, confined by sampling density, current atmospheric CO_2 inversions only provide reliable estimates at relatively coarse spatial resolutions (Byrne et al., 2023). The process-based TBMs, which take the physical process of energy, carbon, and water cycle into account, have become an important tool for studying ecosystems carbon budgets (White et al., 2000). Nevertheless, TBM-based flux estimation suffers considerable uncertainty arising from model structure, model parameterization processes, and driving data (Foster et al., 2024; Huntzinger et al., 2012), and lacks effective constraint from multi-source observations (Ciais et al., 2022). Recently, the rapid development of machine learning (ML) approaches has paved new avenues for modelling the terrestrial carbon cycle. Data-driven ML approaches are straightforward and efficient

https://doi.org/10.5194/essd-2026-418
Preprint. Discussion started: 24 July 2026

for assessing NEE since they allow for easy integration of data and full use of information from various sources (Xiao et al., 2008, 2011, 2014). These methods derive the NEE estimates through spatial extrapolation without making any assumptions about ecosystem patterns (Jung et al., 2019; Xiao et al., 2014).

However, compared with top-down inversions, which assimilate all carbon flux transport pathways, large-scale bottom-up ML-based estimates of NEE contain considerable uncertainty, primarily due to the difficulty of capturing the complex and highly nonlinear responses of NEE to disturbances and climate extremes (Vicca et al., 2014). Characterizing the potential effects of climate change on terrestrial ecosystems is limited by an incomplete understanding of space-time dynamics and the mechanisms regulating ecosystems carbon cycle responses. Observations suggest that the response patterns of ecosystem CO_2 fluxes are influenced by the environment and the memory effects of climate changes, disturbances, and their interactions (Monger et al., 2015). These patterns manifest in the dynamic interactions between biomes and the environment across multiple time scales (Kraft et al., 2019), as terrestrial ecosystems may take months or even years to recover from disturbances caused by climate extremes (Ogle et al., 2015). The memory effects pose challenges to the advancement of research on the carbon cycle and climate change. Only by considering the past vegetation growth status and environmental conditions can we understand how climate change affects the development of current ecosystems on a large scale (Seddon et al., 2016). Moreover, the dependence of carbon cycle dynamics on climate variability is more complex, the IAVs in temperature and precipitation substantially impact carbon flux estimates in terrestrial ecosystems (Piao et al., 2020).

To understand the memory effects of climate extremes on ecosystem carbon fluxes, a considerable amount of research has been conducted (Aubinet et al., 2018; Liu et al., 2018; Shen et al., 2016; Wu et al., 2015). Generally, the link of NEE IAVs to the memory effects of these climate extremes has not been sufficiently characterized by ML-based models. ML methods typically do not directly consider carbon fluxes and stocks at previous time steps, while reflecting the effects of past disturbances to some extent through the use of certain independent datasets (e.g., vegetation indices) (Tao et al., 2020). Thus, these approaches cannot fully represent the inherent temporal interactions of ecosystem carbon cycle processes (Papagiannopoulou et al., 2017). Poor understanding and inadequate representation of memory effects result in substantial uncertainty in estimating regional carbon budget and a considerable difference between top-down inversions and bottom-up estimates (Deng et al., 2013). However, reconciling top-down inversions and bottom-up estimates of NEE is the key way to increase the confidence in quantifying terrestrial ecosystem carbon fluxes at large scales. Therefore, developing the capacity of capturing implicit memory effects in climate and vegetation time series is urgently needed for bottom-up modelling of carbon fluxes.

The Long Short-Term Memory (LSTM) network is a temporal dynamic statistical approach (Besnard et al., 2019; Hochreiter and Schmidhuber, 1997), which effectively addresses long-term dependence issues and thus can incorporate the memory effects of climate change on the terrestrial carbon cycle. LSTM has exhibited an outstanding power in characterizing the memory effects of climate and vegetation on NEE and improving the overall prediction accuracy at the site level (Besnard et al., 2019; Huang et al., 2024; Liu et al., 2023; Ma et al., 2026). As a pioneer such study over large scales, Liu et al. (2023)

https://doi.org/10.5194/essd-2026-418
Preprint. Discussion started: 24 July 2026

proved the importance of the memory effect for assessing IAVs in NEE by conducting an upscaling estimation of global gridded NEE using LSTM. In our previous study, we established LSTM models for NEE prediction by plant function types using flux tower measurements from more than 80 sites and multiple satellite land surface datasets over North America, and confirmed the excellent capacity of LSTM for NEE prediction across various ecosystems, showing obvious advantages over the non-memory Random Forests algorithm, especially in characterizing the IAVs of NEE (Huang et al., 2024). Yet, the capability of LSTM models to characterize the spatiotemporal regimes of NEE on regional scales, particularly with the aid of multi-source satellite land surface data, has not been sufficiently examined. For example, in the study of Liu et al. (2023), only single satellite vegetation variable (i.e., normalized difference vegetation index briefly NDVI) was employed, and how the performance of the upscaling result in capturing the impact of large-scale climate extremes had not been investigated.

In this study, we focus on North America, a region with the most extensive eddy flux observations globally and a relatively well-studied carbon budget. In particular, the substantial carbon uptake in the Midwest Corn Belt has been widely reported as a continental-scale phenomenon since the start of the CarbonTracker inversion (Peters et al., 2007) and during the Mid-Continent Intensive campaign (Schuh et al., 2013), and it has been revisited as a model benchmark feature. However, existing global flux upscaling datasets generally fail to capture this phenomenon. To upscale NEE, we employ an LSTM DL algorithm that fully utilizes in-situ CO_2 flux observations in combination with diverse remote sensing and climate variables. From this, we generate a long-term gridded NEE dataset at a spatial resolution of 0.1° and monthly intervals from 2001 to 2021. The resulting dataset, named MemoryFlux, is publicly available for research purposes. We aim to answer a key scientific question: Does the memory-based deep learning integrating multi-source satellite data benefit the estimation of NEE over North America? An ensemble of flux upscaling datasets and atmospheric inversions are used for comparison and evaluation. This paper particularly focuses on examining the consistency and differences between our product, empirical knowledge, and existing products, as well as assessing whether our new estimate narrows the gap between bottom-up carbon flux upscaling estimates and top-down inversions. Additionally, this study explores the advantages of our estimate in constraining the temporal and spatial characteristics of NEE anomalies caused by climate extremes. We anticipate that MemoryFlux, which incorporates ecosystem memory effects through an LSTM algorithm, provides a more accurate representation of ecosystem carbon fluxes and serves as a valuable resource for investigating terrestrial carbon dynamics and ecosystem–climate interactions.

2 Data and methods

2.1 Datasets

2.1.1 CO_2 eddy covariance flux data

The research area was defined as the primary biomes in North America, focusing on ecoregions from 5° N to 80° N. We used 84 flux sites (Table S1) from FLUXNET2015 (Pastorello et al., 2020) and the AmeriFlux network (Novick et al., 2018),

https://doi.org/10.5194/essd-2026-418
Preprint. Discussion started: 24 July 2026

integrating them with various remote sensing and climate reanalysis data. The target variable of this study was monthly average NEE (g C m^{-2} day^{-1}). The database encompassed the key 10 terrestrial vegetation biomes in North America (Fig. 1), as categorized by the International Geosphere-Biosphere Program (IGBP). These included evergreen needleleaf forest (ENF), deciduous broadleaf forest (DBF), mixed forest (MF), cropland (CRO), grassland (GRA), woody savanna (WSA), open shrubland (OSH), closed shrubland (CSH), savanna (SAV), and permanent wetland (WET).

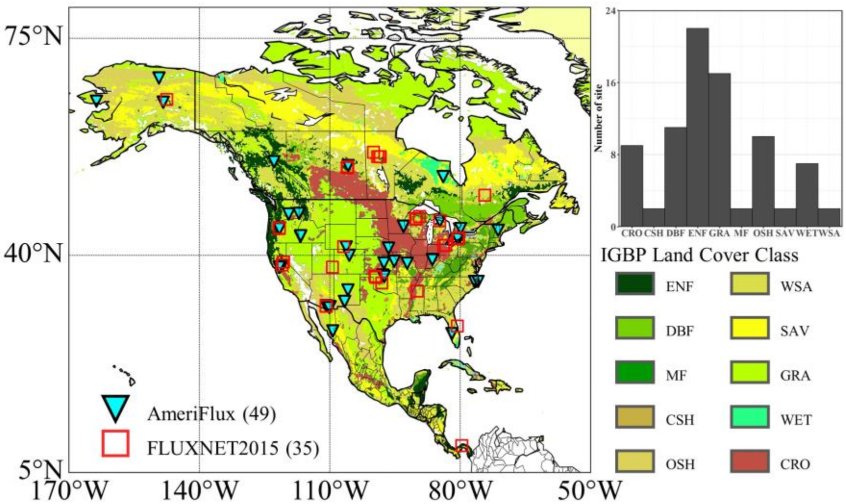

Figure 1. Distribution of the eddy covariance flux towers used in this study. The background information reveals the land cover types across North America, derived from the MCD12C1 dataset. MODIS Land Cover Type Product (MCD12C1) © NASA and U.S. Geological Survey.

2.1.2 Climate reanalysis data

Information about the predictive features used in this study for upscaling NEE is listed in Table 1. These variables were selected to match the climate and environmental drivers at the site level (Huang et al., 2024). We extracted seven environmental relevant predictors from the ERA5-Land dataset, including downward shortwave radiation (DSR), air temperature (TA), dew point temperature (Td), 10m u-component of wind (U10), 10m v-component of wind (V10), soil water content (SWC), and precipitation (P). The dataset is the land component of the fifth generation of European Reanalysis (ERA5) (Muñoz-Sabater et al., 2021), developed by the Copernicus Climate Service at the European Centre for Medium-Range Weather Forecasts. This climate reanalysis data integrated various data sources including both remote sensing observations and ground-based measurements, ultimately providing monthly data at 0.1° resolution.

https://doi.org/10.5194/essd-2026-418
Preprint. Discussion started: 24 July 2026

Table 1. Basic information about the predictive datasets used in this study.

Product	Spatial Resolution	Temporal Resolution	Source	Reference
downward shortwave radiation				
air temperature				
dew point temperature				
10m u-component	0.1°	Monthly	ERA5-Land reanalysis	(Muñoz-Sabater et al., 2021)
10m v-component				
soil water content				
precipitation				
DEM	30m	Single	ALOS	(Takaku et al., 2020)
SIF	0.05°	Monthly	GOSIF	(Li and Xiao, 2019)
NDVI	0.1°	Monthly	MODIS	(Xiong et al., 2023)
LAI	0.1°	8-daily	GLASS	(Liang et al., 2021)
FAPAR				

The U10 and V10 components derived from the ERA5-Land dataset were used to reconstruct wind speed (WS) as the predictive variable for NEE:

$$WS = \sqrt{(U10)^2 + (V10)^2} \tag{1}$$

According to Eq. (2) to Eq. (6), the vapor pressure deficit (VPD) was calculated using the TA and Td retrieved from ERA5-Land:

$$VPD = SVP - AVP \tag{2}$$

where SVP and AVP represent the saturated and actual vapor pressure (hPa), respectively. These values can be computed using the following equations:

$$SVP = 6.112 \times f_w \times exp\left(\frac{17.67T}{T + 243.5}\right) \tag{3}$$

$$AVP = 6.112 \times f_w \times exp\left(\frac{17.67T_d}{T_d + 243.5}\right) \tag{4}$$

$$f_w = 1 + 7 \times 10^{-4} + 3.46 \times 10^{-6} P_{mst} \tag{5}$$

$$P_{mst} = P_{msl} \times \left(\frac{T + 273.16}{T + 273.16 + 0.0065Z}\right)^{5.625} \tag{6}$$

where T is the air temperature (°C), while T_d denotes the dew point temperature (°C). P_{mst} and P_{msl} represent the air pressure (hPa) and the air pressure at the mean sea level (1013.25 hPa), respectively. Z represents the altitude (m) and was provided by the Advanced Land Observing Satellite (ALOS) (Tadono et al., 2016). The 30m data was resampled to 0.1° to

https://doi.org/10.5194/essd-2026-418
Preprint. Discussion started: 24 July 2026

align with the resolution of the ERA5-Land reanalysis dataset. Thereby, monthly VPD values with consistent spatial and temporal coverage were generated.

2.1.3 Satellite data

We further selected remote sensing variables to represent the growth status of vegetation. The NDVI was utilized in this study, which can indicate disturbance by displaying spectral browning signals linked to drought, harvesting, and fire (Myers-Smith et al., 2020). We employed the new global seamless 0.1°, monthly NDVI product, which was derived from Moderate Resolution Imaging Spectroradiometer (MODIS) surface reflectance data using an LSTM network method (Xiong et al., 2023). This product enables long-term vegetation monitoring on a global spatial scale.

Two of the MODIS-based Global Land Surface Satellite (GLASS) product suites (Liang et al., 2021) were used, the leaf area index (LAI) and the fraction of absorbed photosynthetically active radiation (FAPAR). These components have a 0.1° resolution and 8-day intervals covering from 2000 to 2021. To match the temporal resolution of monthly NEE, we generated monthly composites by averaging the 8-day values. For 8-day windows spanning two months, the values were allocated to each month by weighting them according to the number of days within that month.

We also represented the space-time variations of NEE by incorporating novel satellite datasets. Solar-induced chlorophyll fluorescence (SIF) had brought considerable advancement in measuring terrestrial photosynthesis and was reported to have a strong correlation with NEE changes (Huang et al., 2024; Shiga et al., 2018). We employed the monthly Global Orbiting Carbon Observatory-2 (OCO-2) based SIF (GOSIF), a reconstructed SIF dataset with a high resolution (0.05°), developed using OCO-2 SIF, MODIS vegetation index, and MERRA-2 reanalysis data (Li and Xiao, 2019). Subsequently, we resampled the SIF data to a 0.1° resolution using the averaging approach.

The pattern of individual pixel in the MCD12C1 land cover time series from 2001 to 2021 was processed to assign the mode land cover class within each 0.05° grid cell, i.e., land cover change was not considered (Jung et al., 2019). This processing step enabled us to generate a static PFT map, which helped minimize the uncertainty caused by classification errors in the MODIS dataset. We further resampled it to a 0.1° spatial sampling interval employing the major interpolation method.

2.1.4 NEE data products for comparison

Due to the sparse distribution of EC flux towers and the mismatch between product grids and tower footprints, spatial validation of our upscaled dataset requires comparison with published large-scale carbon flux products. Top-down inversions infer surface fluxes directly from CO_2 measurements, thereby integrating all carbon release and uptake processes. This makes them particularly effective at capturing large-scale seasonal and interannual variations, and thus they serve as indispensable benchmarks for evaluating bottom-up products. We selected two authoritative monthly inversion datasets: the OCO-2 Model Inter-comparison Project (MIP) (Byrne et al., 2023) and CarbonTracker (Peters et al., 2007). We used the "LNLGIS" version of the OCO-2 v10 MIP ensemble mean, which had 1° estimates of CO_2 fluxes from 2015 to 2020. To ensure consistency with bottom-up estimates, fire impacts in the OCO-2 v10 MIP were further removed in this study by

https://doi.org/10.5194/essd-2026-418
Preprint. Discussion started: 24 July 2026

Open Access Earth System Science Data Discussions

excluding the fire emissions dataset provided by the National Oceanic and Atmospheric Administration (NOAA) CarbonTracker. Additionally, we included the latest version of CarbonTracker, CT2022 (Jacobson et al., 2023;Peters et al., 2007), developed by NOAA, which provided 1° global estimates of land–atmosphere CO_2 fluxes for 2001–2020 and already excluded fire impacts in its published product.

We also compared our estimates with representative ML-based bottom-up NEE products at both regional and global scales. We collected the regional EC-MOD2012 dataset for North America at 1-km spatial and 8-day temporal resolution for 2000–2012, which was derived from EC flux measurements and MODIS observations (Xiao et al., 2014). For global NEE estimates, we used the FLUXCOM 2020 ensemble products (RS+CRUJRA1.1, 2001–2017; RS+ERA5, 2001–2018) developed by the Max Planck Institute for Biogeochemistry (MPI-BGC) (Jung et al., 2019). The FLUXCOM 2020 ensembles were among the most authoritative global upscaled products, offering 0.5° monthly NEE estimates with broad spatial coverage and continuous temporal records. FLUXCOM-X, the latest generation of FLUXCOM products, provided global 0.05° NEE estimates (2001–2021) with improved methodology and data integration, and was therefore included in our comparison as well (Nelson et al., 2024). We also included NIES2020 (1999–2019, 0.1° every 10 days) from the National Institute for Environmental Studies, Japan. Unlike FLUXCOM, which relied on static PFTs, NIES2020 derived PFT information from LAI-based variables, thereby improving the representation of spatial heterogeneity and enhancing model generalization across ecosystems (Zeng et al., 2020).

These complementary datasets provided a diverse comparison framework, covering regional to global upscaled products and atmospheric inversion results. Comparing our product with these datasets allowed us to cross-validate the effectiveness of the LSTM-based product, evaluate whether it can more accurately reproduce reported empirical knowledge, enhance consistency with atmospheric inversions, and demonstrate stronger robustness in capturing regional-scale NEE spatiotemporal features.

2.2 The LSTM model for NEE upscaling

Traditional non-memory-based models do not directly account for the time-series characteristics of the input data; that is, they lack a dedicated built-in architecture to handle the dependencies between the target variable at the current time and the historical predictive variables. They make independent predictions at each moment and do not utilize memory-based information. The dynamic statistical model, Long Short-Term Memory (LSTM) network (Hochreiter and Schmidhuber, 1997), can use previous variable data of a certain look-back window as input to predict the NEE output at the current time. NEE is a variable influenced by multiple factors, such as climate and environment. Considering that this influence changes over time, it is essential to predict NEE using historical data that capture its response to climate and disturbance conditions over specific periods.

In our previous work, we used the LSTM model to simulate NEE and its IAVs at the site level by linking monthly CO_2 fluxes with environmental and vegetation predictors (Huang et al., 2024). The model was trained with a six-month look-back window to predict the current NEE, enabling it to capture temporal dependencies in vegetation dynamics and meteorological

https://doi.org/10.5194/essd-2026-418
Preprint. Discussion started: 24 July 2026

conditions. This window length corresponds to the empirical memory effect of most ecosystems reported by Liu et al. (2023) and was further validated to provide good predictive performance at the site scale (Huang et al., 2024; Ma et al., 2026). Key input data included environmental variables (TA, WS, P, DSR, SWC, and VPD) obtained from EC tower observations, as well as vegetation variables derived from remote sensing datasets (NDVI, LAI, FAPAR, and SIF), which were used for site-scale model training. We adopted an improved temporal cross-validation strategy to minimize overfitting and enhance model robustness (Fig. S1). Specifically, the initial 70% of data from each site was assigned to the training set, and the remaining 30% served as an independent testing set. During model training, we further employed nested ten-fold cross-validation to internally validate the training set and optimize model hyperparameters using a combination of early stopping and grid search (Bergstra and Bengio, 2012). This design effectively reduced the risk of data leakage and enhanced the model's generalization to unseen data while strictly maintaining the independence of the training, validation, and testing datasets. Loss curves (Fig. S2) confirmed the robustness of the LSTM models.

Building on this foundation, we currently applied the LSTM framework to regional-scale carbon flux upscaling across North America. Remote sensing and meteorological reanalysis gridded datasets were processed into time series of predictor variables for each pixel, which were then input into the corresponding PFT-specific LSTM models. This approach enabled monthly NEE predictions at 0.1° spatial resolution. Predictions were generated for ten PFTs (ENF, DBF, MF, CRO, GRA, WSA, OSH, CSH, SAV, and WET) derived from our site-level input decomposition. For the PFT (SAV), we did not use SWC as a predictor owing to the unavailability of site SWC data. Despite this, the LSTM model still demonstrated considerable performance (R^2 = 0.83) (Fig. S3).

3 Results

3.1 Spatial patterns of NEE in North America

Figure 2 illustrated the spatial patterns of NEE from MemoryFlux as long-term averages over 2001–2021. The use of long-term averages highlighted the typical distribution of NEE while minimizing the influence of interannual variations. Annually, the strongest carbon uptake was observed in the southeastern United States, followed by the northern Pacific Coast and tropical regions, whereas major carbon sources were concentrated in the tundra of northern and central Canada, as well as in the arid central U.S., where precipitation is limited. During the peak growing seasons (July–August), the Corn Belt in the Upper Midwest U.S. (Fig. 2b–c) emerged as the dominant carbon uptake. As the peak growing seasons progressed, the spatial extent of strong carbon uptake contracted in August, though it remained largely consistent with the North American Corn Belt. By the end of the peak growing seasons (September), the carbon uptake area further diminished (Fig. 2d). From July to September, CO_2 sources were mainly concentrated in the western U.S. and southwestern Canada, with both the extent and magnitude of carbon sources exhibiting a continuous increase over time.

https://doi.org/10.5194/essd-2026-418
Preprint. Discussion started: 24 July 2026

Open Access Earth System Science Data Discussions

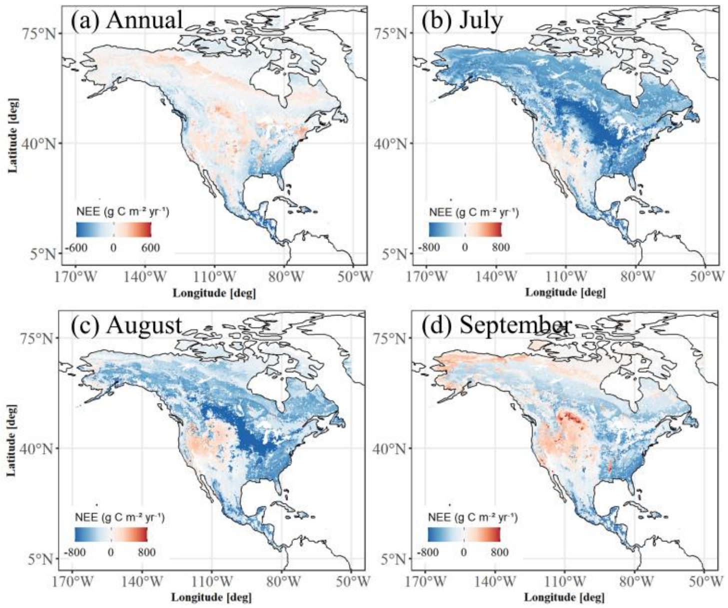

Figure 2. Spatial distribution of the NEE from our MemoryFlux dataset, (a) on an annual basis, (b-c) during peak growing seasons, and (d) in September, averaged over 2001–2021 at 0.1° resolution across North America.

To further evaluate spatial patterns, we compared MemoryFlux with seven other NEE datasets (Fig. 3). On an annual basis, all regional and global ML-based upscaling products, including our MemoryFlux, identified the Southeast as the dominant carbon sink, whereas the OCO-2 v10 MIP and CT2022 inversions indicated the largest uptake in the Midwest Crop Belt area. During peak growing seasons, our estimates closely aligned with OCO-2 v10 MIP, CT2022, and EC-MOD2012, all of which indicated strong seasonal carbon uptake in Midwest U.S. croplands. In contrast, other global flux-upscaling products suggested that the strongest seasonal carbon uptake occurred in the southeastern United States. Latitudinal gradients were generally consistent across datasets, except for the inversions, which exhibited weaker NEE variations along latitude (Fig. 3b and 3d). Furthermore, only the regional NEE estimates from MemoryFlux, EC-MOD2012, and the global FLUXCOM-X consistently identified annual CO_2 sources in northern and central Canada, as well as in the central U.S., and captured growing seasons CO_2 release in the western U.S. and southwestern Canada. Among these datasets, only OCO-2 v10 MIP inversions indicated the northern Pacific Coast and tropical regions as annual carbon sources.

https://doi.org/10.5194/essd-2026-418
Preprint. Discussion started: 24 July 2026

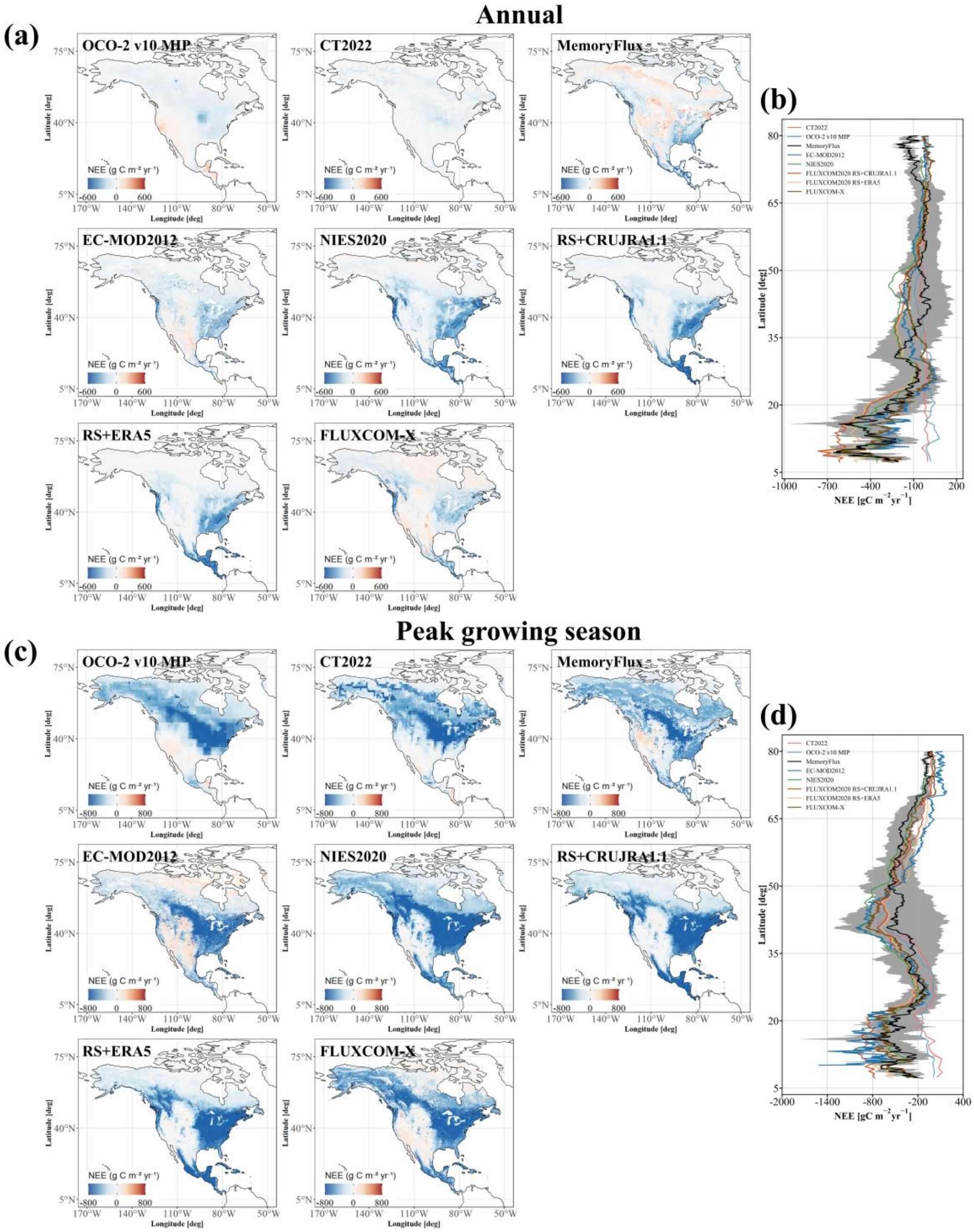

Figure 3. Spatial distribution of NEE in North America on an annual basis and during the peak growing seasons (July–August) derived from OCO-2 v10 MIP, CT2022, MemoryFlux, EC-MOD2012, NIES2020, FLUXCOM2020 RS+CRUJRA1.1, FLUXCOM2020 RS+ERA5, and FLUXCOM-X. The shades around the lines in (b) and (d) represent the range of standard deviation.

https://doi.org/10.5194/essd-2026-418
Preprint. Discussion started: 24 July 2026

Open Access Earth System Science Data Discussions

We further analysed the contributions of major ecoregions to the annual total NEE using the vegetation types classification derived from the Olson et al. (2001), as implemented in the CarbonTracker project (Fig. S4). On average, our estimate indicated that forests/Wooded ecoregions served as the dominant carbon sink in North America, with a mean uptake of -0.76 Pg C yr^{-1}, whereas Grass/Shrubs contributed only marginally, with uptake close to zero. Although all products agreed on the leading role of Forests/Wooded ecosystems as carbon sinks, the magnitude of their contributions varied across datasets: MemoryFlux and FLUXCOM-X attributed more than 85% of the total sink to forests, EC-MOD2012 and other global upscaled products estimated about 75%, while OCO-2 v10 MIP and CT2022 reported substantially lower shares (65% and 38%, respectively). Moreover, only a few products (EC-MOD2012 and FLUXCOM-X) suggested that Grass/Shrubs acted as a weak carbon source.

3.2 Seasonal variations of NEE in North America

To evaluate the seasonal variations of NEE in MemoryFlux, we cross-checked it against other datasets (Fig. 4 and Table S2). This comparison was limited to the period 2015–2017 when all NEE products except EC-MOD2012 were available. The results revealed that MemoryFlux exhibited similar seasonal patterns to other NEE datasets, demonstrating carbon uptake during warm seasons and carbon release in cold. The estimated NEE seasonal cycle well matched the OCO-2 v10 MIP (r = 0.96, $p < 0.001$) and CT2022 inversions (r = 0.97, $p < 0.001$). However, it had weaker net carbon uptake in June, particularly when compared to the estimates by global upscaled products. Notably, all upscaled NEE products exhibited earlier spring onset and later autumn senescence compared with atmospheric inversions. Furthermore, these global upscaled NEE products generally estimated higher carbon uptake than both atmospheric inversions and our estimates, particularly during the growing seasons. NIES2020 exhibited the largest seasonal amplitude in seasonal NEE, particularly in July (Fig. 4a).

https://doi.org/10.5194/essd-2026-418
Preprint. Discussion started: 24 July 2026

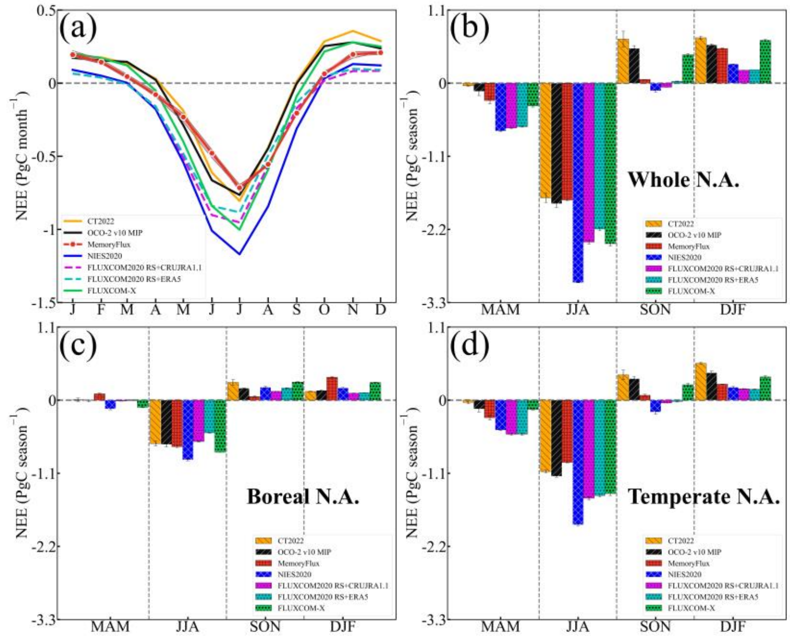

Figure 4. Comparison of the seasonal patterns of MemoryFlux estimated by LSTM models against other products. (a) NEE mean seasonal cycle variations (Pg C month-1) in 2015–2017 derived from MemoryFlux (the shaded area which boundary is standard deviation, the grey line represents the NEE seasonal cycle), NIES2020, OCO-2 v10 MIP, CT2022, FLUXCOM2020 RS+CRUJRA1.1, FLUXCOM2020 RS+ERA5, and FLUXCOM-X. (b-d) Statistics of NEE over the season scale in whole, boreal, and temperate North America. Note that EC-MOD2012 was excluded from this comparison due to the data unavailability.

When comparing these NEE products across the four seasons, consistent patterns emerged but with notable differences in magnitude (Fig. 4b and Table S3). In MAM (March–May) and JJA (June–August), most global upscaled products indicated stronger net carbon uptake than both the atmospheric CO_2 inversions and our estimates. Even the recently updated FLUXCOM-X continued to overestimate JJA carbon uptake, ranking second only to NIES2020. In contrast, MemoryFlux aligned more closely with top-down inversions during MAM and JJA; for example, its JJA uptake was closer to OCO-2 v10 MIP and CT2022 than that of any other upscaling product. During SON (September–November), NEE estimates from FLUXCOM2020 RS+CRUJRA1.1 and NIES2020 indicated net carbon uptake in North America, whereas atmospheric inversions, MemoryFlux, and other globally upscaled estimates suggested net carbon release. In DJF (December–February), FLUXCOM2020 ensemble and NIES2020 exhibited weaker carbon release compared with other products. Consequently, the MemoryFlux dataset, which incorporated memory effects, exhibited improved consistency with atmospheric CO_2 inversions.

We further compared seasonal NEE patterns between the boreal and temperate regions of North America, based on the Transcom partitioning (Fig. 4c–d). Overall, the boreal region showed better agreement, whereas temperate regions were the main contributors to the overestimation of carbon uptake by global upscaling products relative to our estimates and atmospheric inversions. During SON, the net carbon uptake reported by NIES2020 and FLUXCOM2020 RS+CRUJRA1.1 was mainly derived from temperate regions, whereas boreal regions continued to exhibit net carbon release. FLUXCOM-X exhibited uptake in MAM in both regions, whereas CT2022 and MemoryFlux showed this pattern only in the temperate

https://doi.org/10.5194/essd-2026-418
Preprint. Discussion started: 24 July 2026

Open Access Earth System Science Data Discussions

regions. Additionally, MemoryFlux estimated higher carbon release in the boreal region during MAM and DJF, but lower release during SON compared with other products.

3.3 Annual total and interannual variations of NEE in North America

We first investigated the regional total annual NEE and its IAVs in North America across these eight datasets (Fig. 5 and Table S4). The total annual NEE estimated by MemoryFlux ranged between -1.50 and -1.05 Pg C yr^{-1} from 2001 to 2021, which was within the range of NEE estimates by existing models (Table S4). On average, MemoryFlux estimated an annual NEE of -1.27 ± 0.12 Pg C yr^{-1}, which was closer to the top-down inversions (CT2022: -0.70 ± 0.20 Pg C yr^{-1}; OCO-2 v10 MIP: -0.83 ± 0.11 Pg C yr^{-1}) than to the bottom-up flux upscaling products, both regional (EC-MOD2012) and global (NIES2020, FLUXCOM2020 ensemble, and FLUXCOM-X) estimates. Among all datasets, NIES2020 exhibited the largest carbon sink at -3.30 ± 0.22 Pg C yr^{-1}. To further evaluate model performance, we calculated the correlation coefficient (r) of interannual variations in NEE between MemoryFlux and the other products. MemoryFlux showed notable correlations with CT2022 ($r = 0.41$, $p = 0.07$), OCO-2 v10 MIP ($r = 0.70$, $p = 0.12$), EC-MOD2012 ($r = 0.68$, $p < 0.05$), and FLUXCOM-X ($r = 0.69$, $p < 0.05$), whereas it exhibited lower correlations with the other datasets. These results indicated that MemoryFlux, estimated using the LSTM DL approach, effectively captured both the magnitude and IAVs of NEE. In addition, we analysed the long-term trend of NEE in these datasets using the Mann–Kendall test and the Theil–Sen slope method. Due to limited data, no slope was estimated for OCO-2 v10 MIP. The results indicated that MemoryFlux, CT2022, NIES2020, and FLUXCOM-X suggested an overall increase in carbon sinks in North America, whereas EC-MOD2012 and the FLUXCOM 2020 ensemble indicated a slight decrease, although most trends were not statistically significant. Notably, we found that the temperate region was the primary source of divergence in total annual carbon sinks among these NEE products (Fig. S5). Compared with the atmospheric inversions and our MemoryFlux estimates, the upscaled products tended to indicate a higher carbon sink in temperate regions, whereas the boreal region showed relatively good agreement across datasets.

https://doi.org/10.5194/essd-2026-418
Preprint. Discussion started: 24 July 2026

Open Access Earth System Science Data Discussions

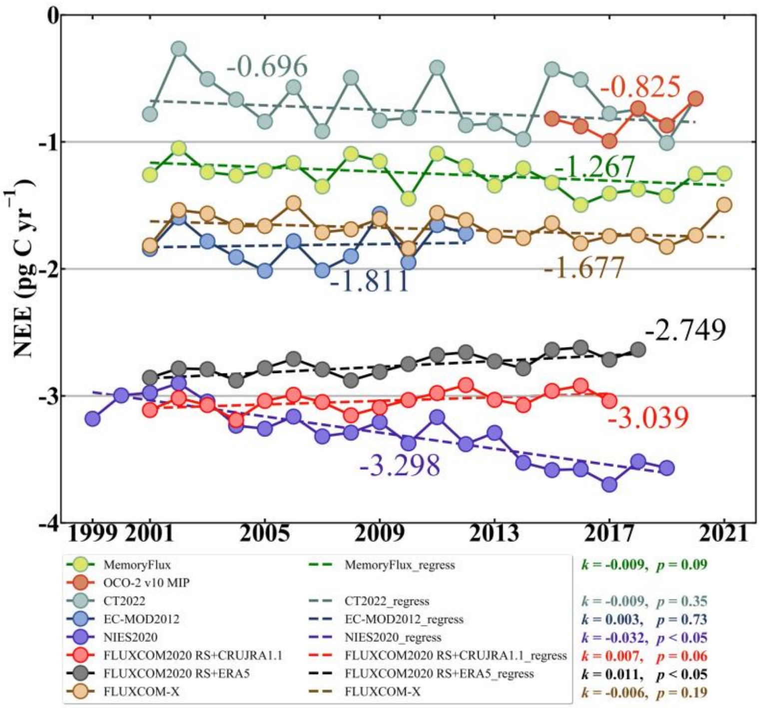

Figure 5. Annual total and interannual variations of North America NEE estimated by OCO-2 v10 MIP, CT2022, MemoryFlux, EC-MOD2012, NIES2020, FLUXCOM2020 RS+CRUJRA, FLUXCOM2020 RS+ERA5, and FLUXCOM-X. The dashed lines represent the long-term trend, calculated using the Mann–Kendall test and the Theil–Sen slope method. Due to the limited data, we did not estimate a slope for OCO-2 v10 MIP.

To evaluate the role of incorporating memory-based climate and environmental information during model training in capturing NEE IAVs, we generated and compared two versions of the LSTM-based NEE dataset: MemoryFlux (with memory) and nonMemoryFlux (without memory). Specifically, MemoryFlux updated its internal state using information observed at past time steps, modelling temporal dependencies and memory effects between the input data and target variables. In contrast, the non-memory variant, nonMemoryFlux, was driven by synchronous explanatory variables to predict the current NEE value. We found that the non-memory models can track the IAVs of NEE reasonably well (r = 0.82, p < 0.001), but clear differences from MemoryFlux still emerged (Fig. 6). In particular, nonMemoryFlux tended to exhibit a stronger increasing trend (-0.013 Pg C yr^{-2}) and to overestimate carbon uptake in recent years (since 2014), when the 2015/16 El Nino events and frequent droughts and heatwaves hit North America, suggesting that it failed to capture the legacy effects of climate extremes on terrestrial ecosystems. The maximum difference reached 186 Tg C yr^{-1} (in 2014; 14.6% of the mean carbon uptake), and the mean absolute difference was 64 Tg C yr^{-1} (5.0% of the mean carbon uptake), highlighting the importance of accounting for memory effects in carbon flux upscaling.

https://doi.org/10.5194/essd-2026-418
Preprint. Discussion started: 24 July 2026

Open Access Earth System Science Data Discussions

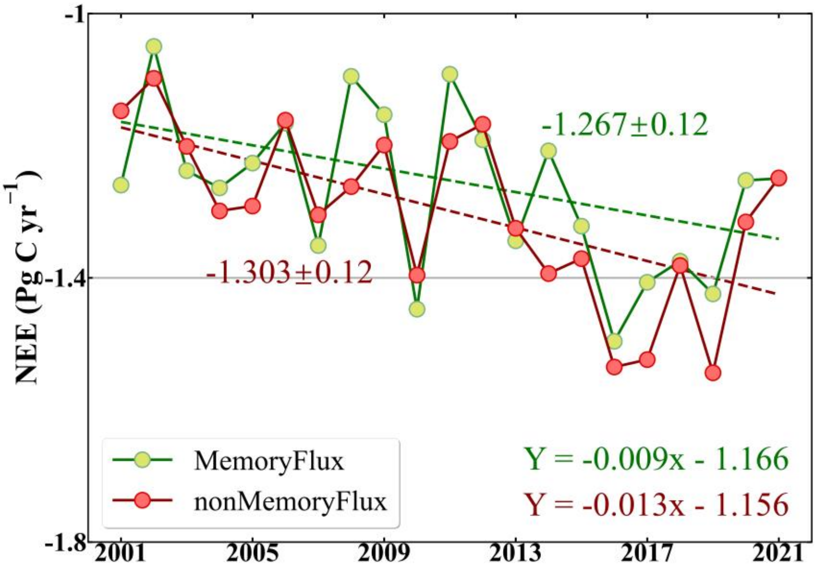

Figure 6. Differences between established LSTM models with memory (MemoryFlux) and those without considering memory (nonMemoryFlux) in revealing the interannual variations of North American NEE. The dashed lines represent the long-term trend, calculated using the Mann–Kendall test and the Theil–Sen slope method.

In addition, we examined the impact of incorporating memory-based information on predicting the seasonality and IAVs of carbon flux at the site scale by comparing the NEE extracted from MemoryFlux and nonMemoryFlux with long-term flux observations across different PFTs (Fig. S6). The results indicated that our estimates were strongly correlated with flux observations at most sites, with substantial site-scale differences between MemoryFlux and nonMemoryFlux. Incorporating memory-based information improved the representation of seasonality and IAVs of NEE, particularly in capturing low values of NEE, whereas the IAVs of NEE captured by nonMemoryFlux were relatively small.

3.4 Monitoring climate extremes impacts on regional NEE

We further explored the performances of the LSTM-based model in indicating NEE IAVs at the grid scale by evaluating its capacity on spatially monitoring the impacts of climate extremes on regional NEE. Given the largest impact typically occurred in the period from June to August (summer, JJA), here we focused our analysis on regional carbon flux anomalies during the summer. Regional NEE anomalies were calculated as the difference between the mean summer NEE during extreme-event years and the multi-year mean summer NEE for each dataset's time span. Soil moisture (SM) anomalies were used to indicate the severity and extent of drought events. The Global Land Evaporation Amsterdam Model (GLEAM) v3.7a datasets at a 0.25° resolution were employed for this study (Martens et al., 2017). Furthermore, regional anomalies of SIF from the GOSIF dataset were utilized to reflect the effects of climate extreme events on vegetation growth. The SIF and SM datasets were used solely as background information to indicate the spatial extent of these extreme events and were not intended as direct proxies for NEE. In the analysis, we chose six events, including the 2011 drought in Mexico and the southern U.S. (Dobler-Morales and Bocco, 2021; Weiss et al., 2012), the 2012 North American drought (Boyer et al., 2013),

https://doi.org/10.5194/essd-2026-418
Preprint. Discussion started: 24 July 2026

the 2013 California drought (Swain et al., 2014), the 2017 flash drought across the northern U.S. and Canadian Prairie (Hoell et al., 2020), the 2019 Midwest American floods (Yin et al., 2020), and the southwestern Northern American drought and associated wildfires during 2020–2021 (Mankin et al., 2021). In these climate extremes, drought and flood conditions caused negative and positive SM anomalies, respectively, and negative SIF anomalies, leading to abnormal CO_2 release from land to the atmosphere, as reflected by positive NEE anomalies.

Figure 7 showed the areas affected by climate extremes across North America for JJA 2011–2013, JJA 2017, JJA 2019, and JJA 2021, based on various datasets. In arid regions, the MemoryFlux dataset exhibited positive NEE anomalies during JJA, which spatially coincided with negative SM and SIF anomalies indicated by environmental proxy datasets. During the 2019 Midwest American floods, SM presented positive anomalies (highlighted by the red rectangle and reversed colour bar), corresponding spatially to negative SIF and positive NEE anomalies. Consistent with the flood-induced affected NEE anomalies range detected by MemoryFlux, the flood map indicated that the Midwest U.S. experienced extensive flooding in 2019, whereas the southern region was only partially affected. The regional NEE anomalies caused by drought and flood events diagnosed by MemoryFlux were supported by the reported range of climate extremes, environmental proxy datasets, and the flood map, suggesting that MemoryFlux effectively captured regional anomalous NEE signals. We further examined the role of incorporating memory-based information in assessing the impacts of climate extremes on NEE. We found that LSTM models that did not incorporate memory effects were less effective than those that did (MemoryFlux) in capturing spatial NEE anomalies associated with climate extremes, such as the 2011–2012 droughts and the 2019 flood event (Fig. 7). This highlighted the superiority of LSTM models with memory effects in representing the impact of climate extremes on carbon fluxes.

https://doi.org/10.5194/essd-2026-418
Preprint. Discussion started: 24 July 2026

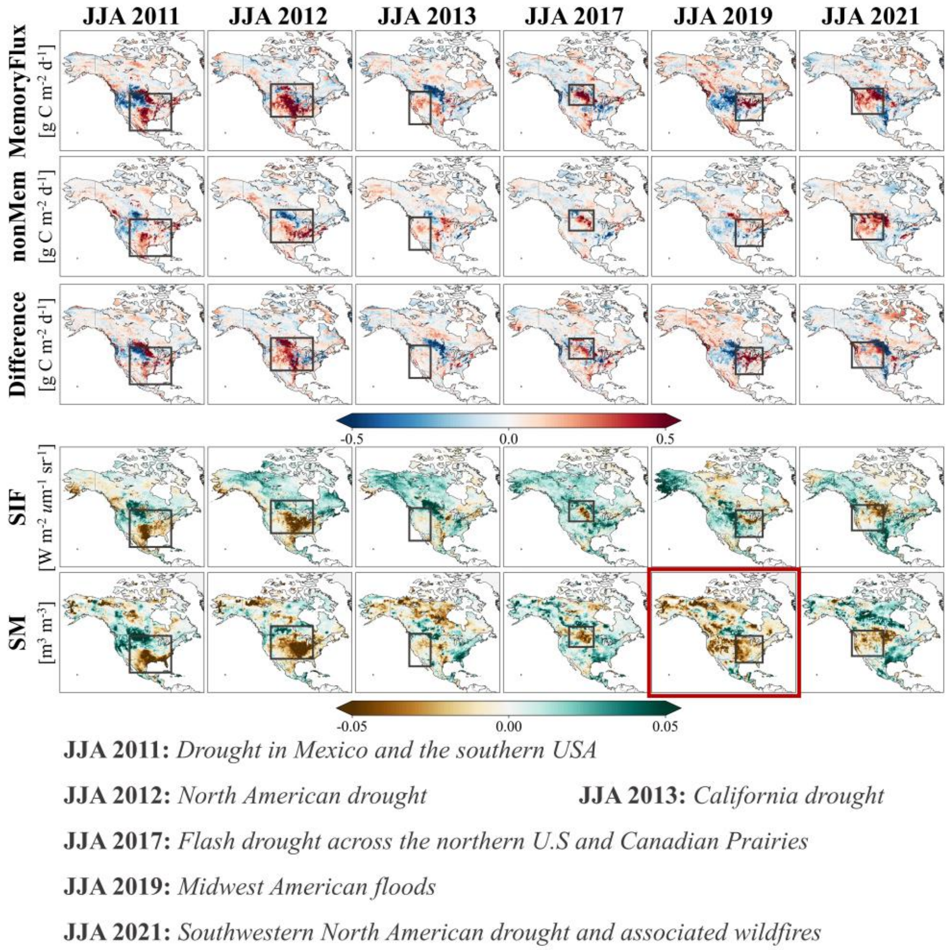

Figure 7. Spatial anomalies of NEE (MemoryFlux and nonMemoryFlux) and environmental proxies (GOSIF and GLEAM dataset) over JJA caused by North American main extreme droughts and floods throughout the study period. The third row represented the difference between the anomalies for MemoryFlux and nonMemoryFlux. The black rectangles indicated the regions that were significantly impacted by climate extreme events. Note that the colour bar was reversed only for the 2019 flood, as indicated by the SM dataset (marked by the red rectangle), to better represent the flooded area, because the SM anomaly was opposite to that observed during drought.

To better understand the advantages of the MemoryFlux dataset in capturing climate extremes-induced spatial anomalies of NEE, we conducted a comparative evaluation with various contemporary datasets (Fig. 8). It can be observed that, in general, the regional flux upscaled estimates by EC-MOD2012 captured the climate extremes–induced regional flux anomalies well, yet they identified a much larger spatial extent of drought impacts. Among the global flux upscaling estimates, NIES2020 and FLUXCOM-X exhibited similar anomaly patterns to MemoryFlux, while both FLUXCOM2020 datasets tended to produce very small anomalies. The MemoryFlux estimate agreed well with the top-down inversion by OCO-2 v10 MIP in indicating the climate extreme events in 2017 and 2019. Furthermore, the MemoryFlux generally aligned with the CT2022 inversion in most events but with spatial differences, possibly due to the limited capacity of in-situ based atmospheric CO_2 inversion in capturing flux anomalies at finer spatial scales. Overall, among these NEE datasets, MemoryFlux demonstrated

https://doi.org/10.5194/essd-2026-418
Preprint. Discussion started: 24 July 2026

robust monitoring capabilities, offering a more accurate representation of regional carbon flux anomalies across all extreme events, even for relatively mild events, such as the 2013 California drought (Fig. 8).

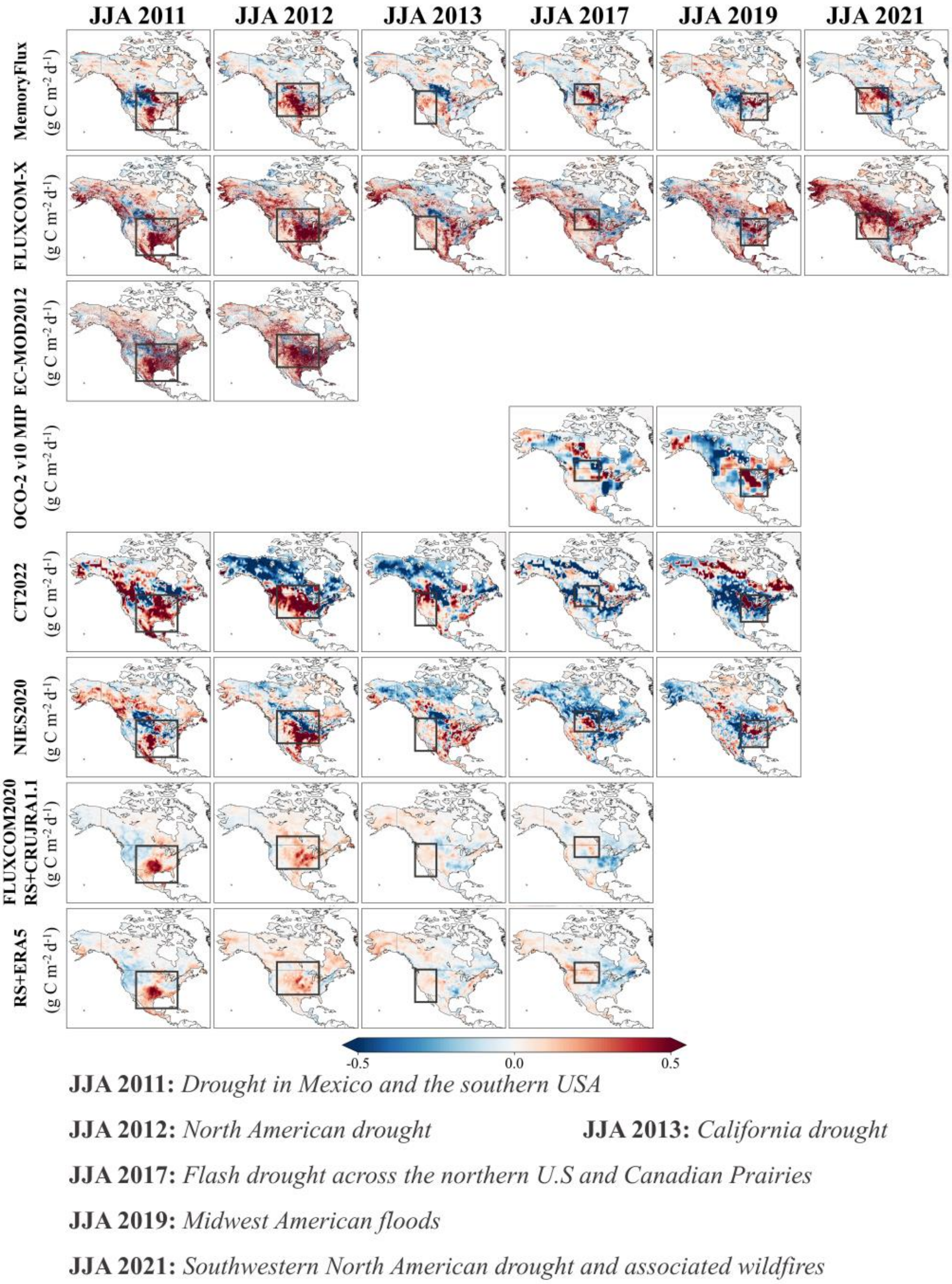

Figure 8. Spatial anomalies of NEE over JJA caused by North American main extreme drought and flood events during the study period, from MemoryFlux, EC-MOD2012, OCO-2 v10 MIP, CT2022, NIES2020, FLUXCOM2020 RS+CRUJRA1.1, FLUXCOM2020 RS+ERA5, and FLUXCOM-X. The black rectangles indicated the regions that were significantly impacted by climate extreme events.

https://doi.org/10.5194/essd-2026-418
Preprint. Discussion started: 24 July 2026

Earth System Science Data
Open Access Discussions

4 Discussion

4.1 North American terrestrial carbon budget: spatial distribution, magnitude, and IAV

Our estimate reasonably identified the spatial features of NEE on an annual basis and during peak growing seasons. Annually, the most spatially extensive carbon sinks were located in the southeastern U.S. and characterized by mild temperatures and ample precipitation, agreeing with previous reports (Guanter et al., 2014; Huntzinger et al., 2012). Additionally, large annual carbon sinks were observed along the North Pacific coast and in tropical regions of North America, where evergreen forests prevailed (Anthoni et al., 2002). During peak growing seasons, the net carbon uptake of croplands was highest in the central and western regions, leading to a large regional carbon uptake in the Midwest Corn Belt (Schuh et al., 2013). Previous researches had demonstrated the peak global photosynthesis in this region (Guanter et al., 2014; Hilton et al., 2017; Mueller et al., 2016). However, the seasonal carbon uptake was transitory. As peak growing seasons advanced, both the spatial extent and magnitude of the strong carbon uptake decreased, because most of the absorbed carbon ended up in crop products that were consumed by humans and livestock or converted into bioethanol. The detection of this seasonal carbon uptake further validated the ability of MemoryFlux to diagnose spatial patterns of NEE. The large carbon sources on an annual basis were observed in the tundra regions of northern and central Canada (Virkkala et al., 2021), as well as in the arid regions of the central U.S. Warming in these regions could lead to the release of soil carbon, thereby accelerating climate change (Natali et al., 2019; Schuur et al., 2021). Many areas in the western U.S. were almost carbon neutral owing to limited vegetation distribution and precipitation (Xiao et al., 2014). Furthermore, according to the carbon sink statistics over boreal and temperate North America, all products indicated that Forests/Wooded biomes were the largest ecosystem carbon sink, and had low disturbance and high productivity (Yadav et al., 2022). Several studies supported forests as the main carbon sink across North America (Kurz et al., 2013; Stinson et al., 2011).

The mean annual total NEE estimated by MemoryFlux was -1.267 ± 0.12 Pg C yr^{-1}, which was closer to top-down atmospheric inversions than to the bottom-up upscaling estimates used for comparison in this study. Several previous studies provide context for our estimates. King et al. (2015) revealed a mean annual net land-atmosphere exchange for North America of -0.890 ± 0.400 Pg C yr^{-1} based on 11 inverse models during 2000–2009. Foster et al. (2024) reported a mean ± 1 standard deviation annual NEE for North America of -0.808 ± 0.476 Pg C yr^{-1} across 8 inverse models from 2007 to 2010. Additionally, our estimate is higher than the recent estimates of -0.606 Pg C yr^{-1} with an uncertainty of ± 75% using a bottom-up approach and of -0.699 Pg C yr^{-1} with an uncertainty of ± 12% using a top-down method over the period 2004–2013 by the Second State of the Carbon Cycle Report (SOCCR2) (Hayes et al., 2018). Our slightly higher NEE estimates compared to those from former top-down inversions may be due to the CO_2 released into the atmosphere from harvested products, fires, inland waters CO_2 fluxes, and many other disturbances not observed at tower sites not being considered in upscaled estimates but typically included in top-down estimates (Ballantyne et al., 2021). Our estimate showed an overall enhanced carbon sink over the past two decades in North America, like CT2022, NIES2020, and FLUXCOM-X, in line with previous studies (Keenan and Williams, 2018; Walker et al., 2021), even though most trends were not statistically significant.

https://doi.org/10.5194/essd-2026-418
Preprint. Discussion started: 24 July 2026

4.2 Capturing climate extremes-induced carbon flux anomalies over North America

The IAVs in atmospheric CO_2 concentration can primarily be ascribed to the response of terrestrial ecosystems carbon fluxes to climate anomalies (Battle et al., 2000). Therefore, in principle, it is convincing to use top-down approaches (e.g., OCO-2 v10 MIP and CT2022) for monitoring carbon anomalies in these events (Venturini, 2022). OCO-2 XCO_2-based inversions (OCO-2 v10 MIP) have been proven to effectively monitor regional carbon flux anomalies caused by climate extremes and have shown significantly better performance compared to in-situ CO_2-based inversions (Chen et al., 2024; He et al., 2023a, b). In this study, the regional NEE anomalies identified by MemoryFlux were well supported by consistent anomalies in NEE estimated from top-down inversions and spatially aligned with climate extreme-driven anomalies in satellite-observed SM and SIF. Notably, MemoryFlux offered a more accurate constraint on carbon flux anomalies over other NEE datasets, particularly those flux upscaling estimates.

Here we further discuss how the implementation of an LSTM architecture in MemoryFlux improved the model estimates of IAVs and climate extremes-induced carbon flux anomalies, i.e., what the roles of considering memory effects and employing critical predictive variables play in this issue. Our findings demonstrated that excluding memory-based information of the historical climate and environmental data from the LSTM models resulted in changes to the predicted spatial and temporal variability of NEE, which showed lower consistency with top-down inversions and contemporary upscaled products. Substantial differences were observed between MemoryFlux and nonMemoryFlux in modelling the seasonality and IAVs of NEE at the pixel scale. The non-memory variant cannot effectively capture the IAVs of NEE (Fig. S6). However, nonMemoryFlux showed a total annual NEE close to that of MemoryFlux. This may be because the difference between MemoryFlux and nonMemoryFlux diminished as the carbon flux was aggregated from the pixel scale to the annual total at the regional scale of North America. This scale effect reduced the differences between the two models. Therefore, the improvement in the magnitude of total NEE in North America can be primarily attributed to the inclusion of additional predictive variables, such as SIF and SWC. In contrast, the effective characterization of NEE IAVs and climate extremes-induced carbon flux anomalies resulted from accounting for the memory-based information of vegetation and the environment.

It should be noted that the nonMemoryFlux estimate also roughly captured the spatial anomalies due to climate extremes in most cases, but exhibited clear underestimation in magnitude and notable discrepancies in spatial extent. This could be explained by the fact that the impact of climate extremes is typically most severe during the concurrent period, while their impact gradually weakens over time (Piao et al., 2019). Therefore, the model, without explicitly considering the memory-based information, captured the major pattern of climate extremes-induced flux anomalies but underestimated the legacy impacts. Another explanation could be the so-called non-memory LSTM run employed some vegetation variables, which may have incorporated some memory effects from previous time steps. MemoryFlux provided more accurate and realistic constraints on NEE anomaly signals at subcontinental regions compared with nonMemoryFlux. The reasonable anomalies in the flux upscaling estimates demonstrate the potential of the LSTM algorithm, which considers memory effects, to constrain

https://doi.org/10.5194/essd-2026-418
Preprint. Discussion started: 24 July 2026

climate extreme impacts using multi-source data time series as inputs.

4.3 Limitations and Future Perspectives

Several limitations exist in this study. Firstly, the accuracy of flux upscaling is tightly linked to the number of observations, meaning that the regions and ecosystems with few observations would suffer from larger uncertainties (see Fig. S2g and S2h) (Zou et al., 2024). We have included as many EC points as possible in North America; however, there are significantly fewer flux towers distributed in the tropical and boreal regions, leading to relatively larger uncertainties in these areas. In some ecosystem types, e.g., SAV, there are only two sites, but it covers a quite large area of North America, which could limit the accuracy of flux estimates for the SAV ecosystem.

Second, the accuracy of PFTs or land cover types may substantially impact the flux upscaling results, as the modelled relationships depend on such classification. How to balance the representativeness of observations across ecosystems is an important issue for upscaling flux from sites to regions. Developing cross-PFT methods could be a promising way, for example replacing them with parameter-environmental relationships as proposed by Famiglietti et al. (2023).

Third, in our upscaled flux modelling, carbon fluxes from crop/wood harvest and river transport were not accounted for due to inner limitations of such methods, which is a common challenge for bottom-up modelling of NEE. This mis-presentation of carbon fluxes could partly explain the remaining gap between ML upscaling estimates and top-down inversions.

Lastly, while this study suggests that the memory effects improve the temporal and spatial characteristics of NEE upscaled estimation, it still overestimates the carbon sink capacity of terrestrial ecosystems compared to top-down atmospheric CO_2 inversions. Some key information affecting NEE IAVs, e.g., biomass, CO_2 fertilization, stand age, and forests management, is not explicitly considered (Xiao et al., 2014), which can contribute to the primary differences between our annual NEE estimates and those derived from atmospheric CO_2 inversions (Yu et al., 2019). In particularly, the variance occurred in the Midwest U.S., which may be linked to the pronounced impact of human management on croplands (Marcolla et al., 2017). Incorporating disturbance history and management information into ML modelling of carbon flux is expected to further narrow the gap in estimated NEE among different methods. Furthermore, although these inversions provide valuable references for seasonal and interannual variations and large-scale carbon budgets, they are not direct measurements of NEE and are subject to uncertainties arising from factors such as atmospheric transport characterization and prior assumptions. Given the limited availability of large-scale flux observations, using these inversions as benchmarks is a practical approach, with future improvements in EC networks and inversion methods expected to further enhance the accuracy and reliability of carbon flux modelling. Therefore, our results are preliminary, and we anticipate that refining our methodology will yield furtherly improved estimates in the future, particularly in terms of seasonality during the non-growing seasons.

5 Code and data availability

The data sets used in this paper are available from open resources. Eddy covariance data for the 35 FLUXNET sites utilized

https://doi.org/10.5194/essd-2026-418
Preprint. Discussion started: 24 July 2026

in this study are available from the FLUXNET2015 data set (https://fluxnet.org/data/fluxnet2015-dataset/). Eddy covariance data for the remaining 47 sites are attained from the AmeriFlux website (https://ameriflux.lbl.gov/data/download-data/). GLASS LAI and FAPAR products are available from http://www.glass.umd.edu/Download.html. NDVI data is available from https://figshare.com/articles/dataset/glass_vi_010_025/22267048. GOSIF is available from http://data.globalecology.unh.edu/data/GOSIF_v2/. ERA5 is available from: https://cds.climate.copernicus.eu/datasets/reanalysis-era5-land-monthly-means?tab=overview. DEM is available from: https://www.eorc.jaxa.jp/ALOS/en/dataset/aw3d30/aw3d30_e.htm. EC-MOD2012 is available at the Global Ecology Data Repository (http://globalecology.unh.edu/data.html). The data for the OCO-2 MIP project are available at https://gml.noaa.gov/ccgg/OCO2_v10mip/. The CarbonTracker2022 carbon flux data is publicly available at https://gml.noaa.gov/aftp/products/carbontracker/co2/. The upscaled FLUXCOM-X products are open access at https://doi.org/10.18160/5NZG-JMJE (Nelson et al., 2023). The MemoryFlux dataset, which incorporated memory effects, along with the main related code, is available at https://doi.org/10.5281/zenodo.20482274 (Huang and He, 2026).

6 Conclusion

This study presents a new regional-scale upscaled estimate of NEE from a bottom-up perspective. The LSTM-based upscaling, combined with selected remote sensing variables and environmental factors, produced results that were consistent with established knowledge and with most NEE products, whereas other datasets exhibited consistency only in specific aspects. MemoryFlux can accurately diagnose the spatial distribution of NEE during peak growing seasons and on an annual basis at a fine resolution of 0.1° × 0.1°. The seasonal cycle of NEE in our estimates well matched the top-down atmospheric CO_2 inversions from OCO-2 v10 MIP (r = 0.96, p < 0.001) and CT2022 (r = 0.97, p < 0.001). The mean annual total and standard deviation of NEE from 2001 to 2021 were -1.267 ± 0.12 Pg C yr^{-1}, which was closer to top-down inversions (OCO-2 v10 MIP and CT2022) than regional (EC-MOD2012) and global (NIES2020, FLUXCOM2020 RS+CRUJRA1.1, FLUXCOM2020 RS+ERA5, and FLUXCOM-X) flux upscaling estimates. Our estimated annual total NEE ranged from -1.50 to -1.05 Pg C yr^{-1}, which was within the range of other estimates. Notably, the estimated IAVs of NEE coincided reasonably well with that of OCO-2 v10 MIP (r = 0.70, p = 0.12) during 2015–2020, CT2022 during 2001–2020 (r = 0.41, p = 0.07), EC-MOD2012 during 2001–2012 (r = 0.68, p < 0.05), and FLUXCOM-X during 2001–2021 (r = 0.69, p < 0.05). The annual total NEE suggests an overall increase in carbon sinks in North America (k = -0.009 Pg C yr^{-2}, p = 0.09), although the trend is not statistically significant. Moreover, MemoryFlux effectively identified all NEE anomalies caused by droughts in 2011–2013, 2017, 2020–2021, as well as the 2019 Midwest floods. When the memory effect was excluded during model training, the spatial and temporal variability of NEE changed pronouncedly, showing lower consistency with top-down inversions and other upscaled products, particularly at smaller scales.

Therefore, MemoryFlux leads to substantial improvements in both spatial and temporal characteristics of NEE estimates over North America, particularly on the IAVs of NEE associated with climate extremes, thereby minimizing the discrepancy

https://doi.org/10.5194/essd-2026-418
Preprint. Discussion started: 24 July 2026

between bottom-up estimates and top-down inversions. This represents a crucial advancement towards robust regional carbon budget estimation.

Author contributions

CH: data curation, formal analysis, investigation, methodology, software, validation, visualization, and writing: original draft. WH: conceptualization, funding acquisition, methodology, project administration, resources, supervision, validation, and writing: review and editing. BB: conceptualization, methodology, and writing: review and editing. NN: conceptualization and writing: review and editing. JX: conceptualization, formal analysis, and writing: review and editing. HY: conceptualization and writing: review and editing. PC: formal analysis and writing: review and editing. SW, XL, HM, PX, MZ, HC, and WJ: writing: review and editing. All authors contributed to reviewing and editing the final version of the manuscript.

Competing interests

Some authors are members of the editorial board of Earth System Science Data.

Acknowledgements

J.X. is supported by University of New Hampshire via Bridge Support. B.B.'s research was carried out at the Jet Propulsion Laboratory, California Institute of Technology, under a contract with the National Aeronautics and Space Administration (80NM0018D0004). We acknowledge FLUXNET and AmeriFlux for providing the flux tower data. CarbonTracker CT2022 results were provided by NOAA GML, Boulder, Colorado, USA. OCO-2 v10 MIP was provided by the NOAA/ESRL Global Monitoring Laboratory. We sincerely thank MPI-BGC and NIES for sharing the FLUXCOM2020 and NIES2020 flux datasets, respectively. We also sincerely acknowledge Shunlin Liang's group for sharing GLASS LAI and FAPAR data.

Financial support

This research is funded by the National Natural Science Foundation of China (grant no. 42277453) and the Basic Research Program of Qinghai Province (grant no. 2025-ZJ-737).

https://doi.org/10.5194/essd-2026-418
Preprint. Discussion started: 24 July 2026

References

Anthoni, P. M., Unsworth, M. H., Law, B. E., Irvine, J., Baldocchi, D. D., Tuyl, S. V., and Moore, D.: Seasonal differences in carbon and water vapor exchange in young and old-growth ponderosa pine ecosystems, Agricultural and Forest Meteorology, 111, 203–222, https://doi.org/10.1016/S0168-1923(02)00021-7, 2002.

Aubinet, M., Hurdebise, Q., Chopin, H., Debacq, A., De Ligne, A., Heinesch, B., Manise, T., and Vincke, C.: Inter-annual variability of Net Ecosystem Productivity for a temperate mixed forest: A predominance of carry-over effects?, Agricultural and Forest Meteorology, 262, 340–353, https://doi.org/10.1016/j.agrformet.2018.07.024, 2018.

Ballantyne, A. P., Liu, Z., Anderegg, W. R., Yu, Z., Stoy, P., Poulter, B., Vanderwall, J., Watts, J., Kelsey, K., and Neff, J.: Reconciling carbon-cycle processes from ecosystem to global scales, Frontiers in Ecol & Environ, 19, 57–65, https://doi.org/10.1002/fee.2296, 2021.

Battle, M., Bender, M. L., Tans, P. P., White, J. W. C., Ellis, J. T., Conway, T., and Francey, R. J.: Global Carbon Sinks and Their Variability Inferred from Atmospheric O2 and δ13C, Science, 287, 2467–2470, https://doi.org/10.1126/science.287.5462.2467, 2000.

Bergstra, J. and Bengio, Y.: Random search for hyper-parameter optimization, J. Mach. Learn. Res., 13, 281–305, 2012.

Besnard, S., Carvalhais, N., Arain, M. A., Black, A., Brede, B., Buchmann, N., Chen, J., Clevers, J. G. P. W., Dutrieux, L. P., Gans, F., Herold, M., Jung, M., Kosugi, Y., Knohl, A., Law, B. E., Paul-Limoges, E., Lohila, A., Merbold, L., Roupsard, O., Valentini, R., Wolf, S., Zhang, X., and Reichstein, M.: Memory effects of climate and vegetation affecting net ecosystem CO_2 fluxes in global forests, PLOS ONE, 14, e0211510, https://doi.org/10.1371/journal.pone.0211510, 2019.

Boyer, J. S., Byrne, P., Cassman, K. G., Cooper, M., Delmer, D., Greene, T., Gruis, F., Habben, J., Hausmann, N., Kenny, N., Lafitte, R., Paszkiewicz, S., Porter, D., Schlegel, A., Schussler, J., Setter, T., Shanahan, J., Sharp, R. E., Vyn, T. J., Warner, D., and Gaffney, J.: The U.S. drought of 2012 in perspective: A call to action, Global Food Security, 2, 139–143, https://doi.org/10.1016/j.gfs.2013.08.002, 2013.

Byrne, B., Wunch, D., Jones, D. B. A., Strong, K., Deng, F., Baker, I., Köhler, P., Frankenberg, C., Joiner, J., Arora, V. K., Badawy, B., Harper, A. B., Warneke, T., Petri, C., Kivi, R., and Roehl, C. M.: Evaluating GPP and Respiration Estimates Over Northern Midlatitude Ecosystems Using Solar-Induced Fluorescence and Atmospheric CO_2 Measurements, Journal of Geophysical Research: Biogeosciences, 123, 2976–2997, https://doi.org/10.1029/2018JG004472, 2018.

Byrne, B., Jones, D. B. A., Strong, K., Polavarapu, S. M., Harper, A. B., Baker, D. F., and Maksyutov, S.: On what scales can GOSAT flux inversions constrain anomalies in terrestrial ecosystems?, Atmospheric Chemistry and Physics, 19, 13017–13035, https://doi.org/10.5194/acp-19-13017-2019, 2019.

Byrne, B., Baker, D. F., Basu, S., Bertolacci, M., Bowman, K. W., Carroll, D., Chatterjee, A., Chevallier, F., Ciais, P., Cressie, N., Crisp, D., Crowell, S., Deng, F., Deng, Z., Deutscher, N. M., Dubey, M. K., Feng, S., García, O. E., Griffith, D. W. T., Herkommer, B., Hu, L., Jacobson, A. R., Janardanan, R., Jeong, S., Johnson, M. S., Jones, D. B. A., Kivi, R., Liu, J., Liu, Z., Maksyutov, S., Miller, J. B., Miller, S. M., Morino, I., Notholt, J., Oda, T., O'Dell, C. W., Oh, Y.-S., Ohyama, H.,

https://doi.org/10.5194/essd-2026-418
Preprint. Discussion started: 24 July 2026

Open Access Earth System Science Data Discussions

Patra, P. K., Peiro, H., Petri, C., Philip, S., Pollard, D. F., Poulter, B., Remaud, M., Schuh, A., Sha, M. K., Shiomi, K., Strong, K., Sweeney, C., Té, Y., Tian, H., Velazco, V. A., Vrekoussis, M., Warneke, T., Worden, J. R., Wunch, D., Yao, Y., Yun, J., Zammit-Mangion, A., and Zeng, N.: National CO_2 budgets (2015–2020) inferred from atmospheric CO_2 observations in support of the global stocktake, Earth System Science Data, 15, 963–1004, https://doi.org/10.5194/essd-15-963-2023, 2023.

Chen, H., He, W., Liu, J., Nguyen, N. T., Chevallier, F., Yang, H., Lv, Y., Huang, C., Rödenbeck, C., Miller, S. M., Jiang, F., Liu, J., Johnson, M. S., Philip, S., Liu, Z., Zeng, N., Basu, S., and Baker, D. F.: Satellite-detected large CO_2 release in southwestern North America during the 2020–2021 drought and associated wildfires, Environ. Res. Lett., 19, 054047, https://doi.org/10.1088/1748-9326/ad3cf7, 2024.

Ciais, P., Bastos, A., Chevallier, F., Lauerwald, R., Poulter, B., Canadell, J. G., Hugelius, G., Jackson, R. B., Jain, A., Jones, M., Kondo, M., Luijkx, I. T., Patra, P. K., Peters, W., Pongratz, J., Petrescu, A. M. R., Piao, S., Qiu, C., Von Randow, C., Regnier, P., Saunois, M., Scholes, R., Shvidenko, A., Tian, H., Yang, H., Wang, X., and Zheng, B.: Definitions and methods to estimate regional land carbon fluxes for the second phase of the REgional Carbon Cycle Assessment and Processes Project (RECCAP-2), Geoscientific Model Development, 15, 1289–1316, https://doi.org/10.5194/gmd-15-1289-2022, 2022.

Deng, F., Chen, J. M., Pan, Y., Peters, W., Birdsey, R., McCullough, K., and Xiao, J.: The use of forest stand age information in an atmospheric CO_2 inversion applied to North America, Biogeosciences, 10, 5335–5348, https://doi.org/10.5194/bg-10-5335-2013, 2013.

Dobler-Morales, C. and Bocco, G.: Social and environmental dimensions of drought in Mexico: An integrative review, International Journal of Disaster Risk Reduction, 55, 102067, https://doi.org/10.1016/j.ijdrr.2021.102067, 2021.

Famiglietti, C. A., Worden, M., Quetin, G. R., Smallman, T. L., Dayal, U., Bloom, A. A., Williams, M., and Konings, A. G.: Global net biome CO_2 exchange predicted comparably well using parameter–environment relationships and plant functional types, Global Change Biology, 29, 2256–2273, https://doi.org/10.1111/gcb.16574, 2023.

Foster, K. T., Sun, W., Shiga, Y. P., Mao, J., and Michalak, A. M.: Multiscale assessment of North American terrestrial carbon balance, Biogeosciences, 21, 869–891, https://doi.org/10.5194/bg-21-869-2024, 2024.

Friedlingstein, P., Jones, M. W., O'Sullivan, M., Andrew, R. M., Bakker, D. C. E., Hauck, J., Le Quéré, C., Peters, G. P., Peters, W., Pongratz, J., Sitch, S., Canadell, J. G., Ciais, P., Jackson, R. B., Alin, S. R., Anthoni, P., Bates, N. R., Becker, M., Bellouin, N., Bopp, L., Chau, T. T. T., Chevallier, F., Chini, L. P., Cronin, M., Currie, K. I., Decharme, B., Djeutchouang, L. M., Dou, X., Evans, W., Feely, R. A., Feng, L., Gasser, T., Gilfillan, D., Gkritzalis, T., Grassi, G., Gregor, L., Gruber, N., Gürses, Ö., Harris, I., Houghton, R. A., Hurtt, G. C., Iida, Y., Ilyina, T., Luijkx, I. T., Jain, A., Jones, S. D., Kato, E., Kennedy, D., Klein Goldewijk, K., Knauer, J., Korsbakken, J. I., Körtzinger, A., Landschützer, P., Lauvset, S. K., Lefèvre, N., Lienert, S., Liu, J., Marland, G., McGuire, P. C., Melton, J. R., Munro, D. R., Nabel, J. E. M. S., Nakaoka, S.-I., Niwa, Y., Ono, T., Pierrot, D., Poulter, B., Rehder, G., Resplandy, L., Robertson, E., Rödenbeck, C., Rosan, T. M., Schwinger, J., Schwingshackl, C., Séférian, R., Sutton, A. J., Sweeney, C., Tanhua, T., Tans, P. P., Tian, H., Tilbrook, B., Tubiello, F., van der Werf, G. R., Vuichard, N., Wada, C., Wanninkhof, R., Watson, A. J., Willis, D., Wiltshire, A. J., Yuan, W., Yue, C., Yue, X., Zaehle, S., and Zeng, J.: Global Carbon Budget 2021, Earth System Science Data, 14, 1917–2005, https://doi.org/10.5194/essd-14-1917-2022, 2022.

Guanter, L., Zhang, Y., Jung, M., Joiner, J., Voigt, M., Berry, J. A., Frankenberg, C., Huete, A. R., Zarco-Tejada, P., Lee, J.-E., Moran, M. S., Ponce-Campos, G., Beer, C., Camps-Valls, G., Buchmann, N., Gianelle, D., Klumpp, K., Cescatti, A., Baker, J. M., and Griffis, T. J.: Global and time-resolved monitoring of crop photosynthesis with chlorophyll fluorescence, Proceedings of the National Academy of Sciences, 111, E1327–E1333, https://doi.org/10.1073/pnas.1320008111, 2014.

Hayes, D. J., Vargas, R., Alin, S. R., Conant, R. T., Hutyra, L. R., Jacobson, A. R., Kurz, W. A., Liu, S., McGuire, A. D., Poulter, B., and Woodall, C. W.: The North American carbon budget, in: Second State of the Carbon Cycle Report (SOCCR2): A Sustained Assessment Report, edited by: Cavallaro, N., Shrestha, G., Birdsey, R., Mayes, M. A., Najjar, R. G., Reed, S. C., Romero-Lankao, P., and Zhu, Z., U.S. Global Change Research Program, Washington, DC, USA, 71–108, https://doi.org/10.7930/SOCCR2.2018.Ch2, 2018.

He, W., Jiang, F., Ju, W., Byrne, B., Xiao, J., Nguyen, N. T., Wu, M., Wang, S., Wang, J., Rödenbeck, C., Li, X., Scholze, M., Monteil, G., Wang, H., Zhou, Y., He, Q., and Chen, J. M.: Do State-Of-The-Art Atmospheric CO_2 Inverse Models Capture Drought Impacts on the European Land Carbon Uptake?, Journal of Advances in Modeling Earth Systems, 15, e2022MS003150, https://doi.org/10.1029/2022MS003150, 2023a.

He, W., Jiang, F., Ju, W., Chevallier, F., Baker, D. F., Wang, J., Wu, M., Johnson, M. S., Philip, S., Wang, H., Bertolacci, M., Liu, Z., Zeng, N., and Chen, J. M.: Improved Constraints on the Recent Terrestrial Carbon Sink Over China by Assimilating OCO-2 XCO_2 Retrievals, Journal of Geophysical Research: Atmospheres, 128, e2022JD037773, https://doi.org/10.1029/2022JD037773, 2023b.

Hilton, T. W., Whelan, M. E., Zumkehr, A., Kulkarni, S., Berry, J. A., Baker, I. T., Montzka, S. A., Sweeney, C., Miller, B. R., and Elliott Campbell, J.: Peak growing season gross uptake of carbon in North America is largest in the Midwest USA, Nature Clim Change, 7, 450–454, https://doi.org/10.1038/nclimate3272, 2017.

Hochreiter, S. and Schmidhuber, J.: Long Short-Term Memory, Neural Comput, 9, 1735–1780, https://doi.org/10.1162/neco.1997.9.8.1735, 1997.

Hoell, A., Parker, B.-A., Downey, M., Umphlett, N., Jencso, K., Akyuz, F. A., Peck, D., Hadwen, T., Fuchs, B., Kluck, D., Edwards, L., Perlwitz, J., Eischeid, J., Deheza, V., Pulwarty, R., and Bevington, K.: Lessons Learned from the 2017 Flash Drought across the U.S. Northern Great Plains and Canadian Prairies, https://doi.org/10.1175/BAMS-D-19-0272.1, 2020.

Huang, C., He, W., Liu, J., Nguyen, N. T., Yang, H., Lv, Y., Chen, H., and Zhao, M.: Exploring the Potential of Long Short-Term Memory Networks for Predicting Net CO_2 Exchange Across Various Ecosystems With Multi-Source Data, Journal of Geophysical Research: Atmospheres, 129, e2023JD040418, https://doi.org/10.1029/2023JD040418, 2024.

Huang, C. and He, W.: Improved estimation of net ecosystem CO_2 exchange over North America using LSTM-based flux upscaling (2001–2021), Zenodo [data set], https://doi.org/10.5281/zenodo.20482274, 2026.

Huntzinger, D. N., Post, W. M., Wei, Y., Michalak, A. M., West, T. O., Jacobson, A. R., Baker, I. T., Chen, J. M., Davis, K. J., Hayes, D. J., Hoffman, F. M., Jain, A. K., Liu, S., McGuire, A. D., Neilson, R. P., Potter, C., Poulter, B., Price, D., Raczka, B. M., Tian, H. Q., Thornton, P., Tomelleri, E., Viovy, N., Xiao, J., Yuan, W., Zeng, N., Zhao, M., and Cook, R.: North American Carbon Program (NACP) regional interim synthesis: Terrestrial biospheric model intercomparison, Ecological Modelling, 232, 144–157, https://doi.org/10.1016/j.ecolmodel.2012.02.004, 2012.

Jacobson, A. R., Schuldt, K. N., Tans, P., Andrews, A., Miller, J. B., Oda, T., Mund, J., Weir, B., Ott, L., Aalto, T., Abshire, J. B., Aikin, K., Aoki, S., Apadula, F., Arnold, S., et al.: CarbonTracker CT2022, NOAA Global Monitoring Laboratory, https://doi.org/10.25925/Z1GJ-3254, 2023.

Jung, M., Koirala, S., Weber, U., Ichii, K., Gans, F., Camps-Valls, G., Papale, D., Schwalm, C., Tramontana, G., and Reichstein, M.: The FLUXCOM ensemble of global land-atmosphere energy fluxes, Sci Data, 6, 74, https://doi.org/10.1038/s41597-019-0076-8, 2019.

Keenan, T. F. and Williams, C. A.: The Terrestrial Carbon Sink, Annual Review of Environment and Resources, 43, 219–243, https://doi.org/10.1146/annurev-environ-102017-030204, 2018.

King, A. W., Andres, R. J., Davis, K. J., Hafer, M., Hayes, D. J., Huntzinger, D. N., de Jong, B., Kurz, W. A., McGuire, A. D., Vargas, R., Wei, Y., West, T. O., and Woodall, C. W.: North America's net terrestrial CO_2 exchange with the atmosphere 1990–2009, Biogeosciences, 12, 399–414, https://doi.org/10.5194/bg-12-399-2015, 2015.

Kraft, B., Jung, M., Körner, M., Requena Mesa, C., Cortés, J., and Reichstein, M.: Identifying Dynamic Memory Effects on Vegetation State Using Recurrent Neural Networks, Front. Big Data, 2, https://doi.org/10.3389/fdata.2019.00031, 2019.

Kurz, W. A., Shaw, C. H., Boisvenue, C., Stinson, G., Metsaranta, J., Leckie, D., Dyk, A., Smyth, C., and Neilson, E. T.: Carbon in Canada's boreal forest — A synthesis, Environ. Rev., 21, 260–292, https://doi.org/10.1139/er-2013-0041, 2013.

Le Quéré, C., Andrew, R. M., Friedlingstein, P., Sitch, S., Pongratz, J., Manning, A. C., Korsbakken, J. I., Peters, G. P., Canadell, J. G., Jackson, R. B., Boden, T. A., Tans, P. P., Andrews, O. D., Arora, V. K., Bakker, D. C. E., Barbero, L., Becker, M., Betts, R. A., Bopp, L., Chevallier, F., Chini, L. P., Ciais, P., Cosca, C. E., Cross, J., Currie, K., Gasser, T., Harris, I., Hauck, J., Haverd, V., Houghton, R. A., Hunt, C. W., Hurtt, G., Ilyina, T., Jain, A. K., Kato, E., Kautz, M., Keeling, R. F., Klein Goldewijk, K., Körtzinger, A., Landschützer, P., Lefèvre, N., Lenton, A., Lienert, S., Lima, I., Lombardozzi, D., Metzl, N., Millero, F., Monteiro, P. M. S., Munro, D. R., Nabel, J. E. M. S., Nakaoka, S., Nojiri, Y., Padin, X. A., Peregon, A., Pfeil, B., Pierrot, D., Poulter, B., Rehder, G., Reimer, J., Rödenbeck, C., Schwinger, J., Séférian, R., Skjelvan, I., Stocker, B. D., Tian, H., Tilbrook, B., Tubiello, F. N., van der Laan-Luijkx, I. T., van der Werf, G. R., van Heuven, S., Viovy, N., Vuichard, N., Walker, A. P., Watson, A. J., Wiltshire, A. J., Zaehle, S., and Zhu, D.: Global Carbon Budget 2017, Earth System Science Data, 10, 405–448, https://doi.org/10.5194/essd-10-405-2018, 2018.

Li, X. and Xiao, J.: A Global, 0.05-Degree Product of Solar-Induced Chlorophyll Fluorescence Derived from OCO-2, MODIS, and Reanalysis Data, Remote Sensing, 11, 517, https://doi.org/10.3390/rs11050517, 2019.

Liang, S., Cheng, J., Jia, K., Jiang, B., Liu, Q., Xiao, Z., Yao, Y., Yuan, W., Zhang, X., Zhao, X., and Zhou, J.: The Global Land Surface Satellite (GLASS) Product Suite, Bulletin of the American Meteorological Society, 102, E323–E337, https://doi.org/10.1175/BAMS-D-18-0341.1, 2021.

https://doi.org/10.5194/essd-2026-418
Preprint. Discussion started: 24 July 2026

Liu, L., Zhang, Y., Wu, S., Li, S., and Qin, D.: Water memory effects and their impacts on global vegetation productivity and resilience, Sci Rep, 8, 2962, https://doi.org/10.1038/s41598-018-21339-4, 2018.

Liu, W., He, H., Wu, X., Ren, X., Zhang, L., shi, L., Feng, L., Wang, Y., and Lv, Y.: Importance of the memory effect for assessing interannual variation in net ecosystem exchange, Agricultural and Forest Meteorology, 341, 109691, https://doi.org/10.1016/j.agrformet.2023.109691, 2023.

Ma, T., He, W., Fang, S., Xiao, J., Nguyen, N. T., Yang, H., Xu, P., Huang, C., Zhao, M., Liu, S., Lei, X., and Huang, Z.: Temporal Memory Mechanisms and Biome-Specific Drivers of Ecosystem Carbon Flux: Insights From Explainable Deep Learning Modeling, Global Change Biology, 32, e70722, https://doi.org/10.1111/gcb.70722, 2026.

Mankin, J. S., Simpson, I., Hoell, A., Fu, R., Lisonbee, J., Sheffield, A., and Barrie, D.: NOAA Drought Task Force Report on the 2020–2021 Southwestern U.S. Drought, NOAA Drought Task Force, MAPP, and NIDIS, https://doi.org/10.25923/j0rj-an85, 2021.

Marcolla, B., Rödenbeck, C., and Cescatti, A.: Patterns and controls of inter-annual variability in the terrestrial carbon budget, Biogeosciences, 14, 3815–3829, https://doi.org/10.5194/bg-14-3815-2017, 2017.

Martens, B., Miralles, D. G., Lievens, H., van der Schalie, R., de Jeu, R. A. M., Fernández-Prieto, D., Beck, H. E., Dorigo, W. A., and Verhoest, N. E. C.: GLEAM v3: satellite-based land evaporation and root-zone soil moisture, Geoscientific Model Development, 10, 1903–1925, https://doi.org/10.5194/gmd-10-1903-2017, 2017.

Monger, C., Sala, O. E., Duniway, M. C., Goldfus, H., Meir, I. A., Poch, R. M., Throop, H. L., and Vivoni, E. R.: Legacy effects in linked ecological–soil–geomorphic systems of drylands, Frontiers in Ecology and the Environment, 13, 13–19, https://doi.org/10.1890/140269, 2015.

Mueller, N. D., Butler, E. E., McKinnon, K. A., Rhines, A., Tingley, M., Holbrook, N. M., and Huybers, P.: Cooling of US Midwest summer temperature extremes from cropland intensification, Nature Clim Change, 6, 317–322, https://doi.org/10.1038/nclimate2825, 2016.

Muñoz-Sabater, J., Dutra, E., Agustí-Panareda, A., Albergel, C., Arduini, G., Balsamo, G., Boussetta, S., Choulga, M., Harrigan, S., Hersbach, H., Martens, B., Miralles, D. G., Piles, M., Rodríguez-Fernández, N. J., Zsoter, E., Buontempo, C., and Thépaut, J.-N.: ERA5-Land: a state-of-the-art global reanalysis dataset for land applications, Earth System Science Data, 13, 4349–4383, https://doi.org/10.5194/essd-13-4349-2021, 2021.

Myers-Smith, I. H., Kerby, J. T., Phoenix, G. K., Bjerke, J. W., Epstein, H. E., Assmann, J. J., John, C., Andreu-Hayles, L., Angers-Blondin, S., Beck, P. S. A., Berner, L. T., Bhatt, U. S., Bjorkman, A. D., Blok, D., Bryn, A., Christiansen, C. T., Cornelissen, J. H. C., Cunliffe, A. M., Elmendorf, S. C., Forbes, B. C., Goetz, S. J., Hollister, R. D., de Jong, R., Loranty, M. M., Macias-Fauria, M., Maseyk, K., Normand, S., Olofsson, J., Parker, T. C., Parmentier, F.-J. W., Post, E., Schaepman-Strub, G., Stordal, F., Sullivan, P. F., Thomas, H. J. D., Tømmervik, H., Treharne, R., Tweedie, C. E., Walker, D. A., Wilmking, M., and Wipf, S.: Complexity revealed in the greening of the Arctic, Nat. Clim. Chang., 10, 106–117, https://doi.org/10.1038/s41558-019-0688-1, 2020.

https://doi.org/10.5194/essd-2026-418
Preprint. Discussion started: 24 July 2026

Natali, S. M., Watts, J. D., Rogers, B. M., Potter, S., Ludwig, S. M., Selbmann, A.-K., Sullivan, P. F., Abbott, B. W., Arndt, K. A., Birch, L., Björkman, M. P., Bloom, A. A., Celis, G., Christensen, T. R., Christiansen, C. T., Commane, R., Cooper, E. J., Crill, P., Czimczik, C., Davydov, S., Du, J., Egan, J. E., Elberling, B., Euskirchen, E. S., Friborg, T., Genet, H., Göckede, M., Goodrich, J. P., Grogan, P., Helbig, M., Jafarov, E. E., Jastrow, J. D., Kalhori, A. A. M., Kim, Y., Kimball, J. S., Kutzbach, L., Lara, M. J., Larsen, K. S., Lee, B.-Y., Liu, Z., Loranty, M. M., Lund, M., Lupascu, M., Madani, N., Malhotra, A., Matamala, R., McFarland, J., McGuire, A. D., Michelsen, A., Minions, C., Oechel, W. C., Olefeldt, D., Parmentier, F.-J. W., Pirk, N., Poulter, B., Quinton, W., Rezanezhad, F., Risk, D., Sachs, T., Schaefer, K., Schmidt, N. M., Schuur, E. A. G., Semenchuk, P. R., Shaver, G., Sonnentag, O., Starr, G., Treat, C. C., Waldrop, M. P., Wang, Y., Welker, J., Wille, C., Xu, X., Zhang, Z., Zhuang, Q., and Zona, D.: Large loss of CO_2 in winter observed across the northern permafrost region, Nat. Clim. Chang., 9, 852–857, https://doi.org/10.1038/s41558-019-0592-8, 2019.

Nelson, J. A., Walther, S., Jung, M., Gans, F., Kraft, B., Weber, U., Hamdi, Z., Duveiller, G., and Zhang, W.: FLUXCOM-X-BASE, ICOS Carbon Portal [data set], https://doi.org/10.18160/5NZG-JMJE, 2023.

Nelson, J. A., Walther, S., Gans, F., Kraft, B., Weber, U., Novick, K., Buchmann, N., Migliavacca, M., Wohlfahrt, G., Šigut, L., Ibrom, A., Papale, D., Göckede, M., Duveiller, G., Knohl, A., Hörtnagl, L., Scott, R. L., Dušek, J., Zhang, W., Hamdi, Z. M., Reichstein, M., Aranda-Barranco, S., Ardö, J., Op de Beeck, M., Billesbach, D., Bowling, D., Bracho, R., Brümmer, C., Camps-Valls, G., Chen, S., Cleverly, J. R., Desai, A., Dong, G., El-Madany, T. S., Euskirchen, E. S., Feigenwinter, I., Galvagno, M., Gerosa, G. A., Gielen, B., Goded, I., Goslee, S., Gough, C. M., Heinesch, B., Ichii, K., Jackowicz-Korczynski, M. A., Klosterhalfen, A., Knox, S., Kobayashi, H., Kohonen, K.-M., Korkiakoski, M., Mammarella, I., Gharun, M., Marzuoli, R., Matamala, R., Metzger, S., Montagnani, L., Nicolini, G., O'Halloran, T., Ourcival, J.-M., Peichl, M., Pendall, E., Ruiz Reverter, B., Roland, M., Sabbatini, S., Sachs, T., Schmidt, M., Schwalm, C. R., Shekhar, A., Silberstein, R., Silveira, M. L., Spano, D., Tagesson, T., Tramontana, G., Trotta, C., Turco, F., Vesala, T., Vincke, C., Vitale, D., Vivoni, E. R., Wang, Y., Woodgate, W., Yepez, E. A., Zhang, J., Zona, D., and Jung, M.: X-BASE: the first terrestrial carbon and water flux products from an extended data-driven scaling framework, FLUXCOM-X, Biogeosciences, 21, 5079–5115, https://doi.org/10.5194/bg-21-5079-2024, 2024.

Novick, K. A., Biederman, J. A., Desai, A. R., Litvak, M. E., Moore, D. J. P., Scott, R. L., and Torn, M. S.: The AmeriFlux network: A coalition of the willing, Agricultural and Forest Meteorology, 249, 444–456, https://doi.org/10.1016/j.agrformet.2017.10.009, 2018.

Ogle, K., Barber, J. J., Barron-Gafford, G. A., Bentley, L. P., Young, J. M., Huxman, T. E., Loik, M. E., and Tissue, D. T.: Quantifying ecological memory in plant and ecosystem processes, Ecology Letters, 18, 221–235, https://doi.org/10.1111/ele.12399, 2015.

Olson, D. M., Dinerstein, E., Wikramanayake, E. D., Burgess, N. D., Powell, G. V. N., Underwood, E. C., D'amico, J. A., Itoua, I., Strand, H. E., Morrison, J. C., Loucks, C. J., Allnutt, T. F., Ricketts, T. H., Kura, Y., Lamoreux, J. F., Wettengel, W. W., Hedao, P., and Kassem, K. R.: Terrestrial Ecoregions of the World: A New Map of Life on Earth: A new global map of terrestrial ecoregions provides an innovative tool for conserving biodiversity, BioScience, 51, 933–938, https://doi.org/10.1641/0006-3568(2001)051%5B0933:TEOTWA%5D2.0.CO;2, 2001.

Papagiannopoulou, C., Miralles, D. G., Decubber, S., Demuzere, M., Verhoest, N. E. C., Dorigo, W. A., and Waegeman, W.: A non-linear Granger-causality framework to investigate climate–vegetation dynamics, Geoscientific Model Development, 10, 1945–1960, https://doi.org/10.5194/gmd-10-1945-2017, 2017.

Pastorello, G., Trotta, C., Canfora, E., Chu, H., Christianson, D., Cheah, Y.-W., Poindexter, C., Chen, J., Elbashandy, A., Humphrey, M., Isaac, P., Polidori, D., Reichstein, M., Ribeca, A., van Ingen, C., Vuichard, N., Zhang, L., Amiro, B., Ammann, C., Arain, M. A., Ardö, J., Arkebauer, T., Arndt, S. K., Arriga, N., Aubinet, M., Aurela, M., Baldocchi, D., Barr, A., Beamesderfer, E., Marchesini, L. B., Bergeron, O., Beringer, J., Bernhofer, C., Berveiller, D., Billesbach, D., Black, T. A., Blanken, P. D., Bohrer, G., Boike, J., Bolstad, P. V., Bonal, D., Bonnefond, J.-M., Bowling, D. R., Bracho, R., Brodeur, J., Brümmer, C., Buchmann, N., Burban, B., Burns, S. P., Buysse, P., Cale, P., Cavagna, M., Cellier, P., Chen, S., Chini, I., Christensen, T. R., Cleverly, J., Collalti, A., Consalvo, C., Cook, B. D., Cook, D., Coursolle, C., Cremonese, E., Curtis, P. S., D'Andrea, E., da Rocha, H., Dai, X., Davis, K. J., Cinti, B. D., Grandcourt, A. de, Ligne, A. D., De Oliveira, R. C., Delpierre, N., Desai, A. R., Di Bella, C. M., Tommasi, P. di, Dolman, H., Domingo, F., Dong, G., Dore, S., Duce, P., Dufrêne, E., Dunn, A., Dušek, J., Eamus, D., Eichelmann, U., ElKhidir, H. A. M., Eugster, W., Ewenz, C. M., Ewers, B., Famulari, D., Fares, S., Feigenwinter, I., Feitz, A., Fensholt, R., Filippa, G., Fischer, M., Frank, J., Galvagno, M., et al.: The FLUXNET2015 dataset and the ONEFlux processing pipeline for eddy covariance data, Sci Data, 7, 225, https://doi.org/10.1038/s41597-020-0534-3, 2020.

Peters, W., Jacobson, A. R., Sweeney, C., Andrews, A. E., Conway, T. J., Masarie, K., Miller, J. B., Bruhwiler, L. M. P., Pétron, G., Hirsch, A. I., Worthy, D. E. J., van der Werf, G. R., Randerson, J. T., Wennberg, P. O., Krol, M. C., and Tans, P. P.: An atmospheric perspective on North American carbon dioxide exchange: CarbonTracker, Proceedings of the National Academy of Sciences, 104, 18925–18930, https://doi.org/10.1073/pnas.0708986104, 2007.

Piao, S., Liu, Q., Chen, A., Janssens, I. A., Fu, Y., Dai, J., Liu, L., Lian, X., Shen, M., and Zhu, X.: Plant phenology and global climate change: Current progresses and challenges, Global Change Biology, 25, 1922–1940, https://doi.org/10.1111/gcb.14619, 2019.

Piao, S., Wang, X., Wang, K., Li, X., Bastos, A., Canadell, J. G., Ciais, P., Friedlingstein, P., and Sitch, S.: Interannual variation of terrestrial carbon cycle: Issues and perspectives, Global Change Biology, 26, 300–318, https://doi.org/10.1111/gcb.14884, 2020.

Schuh, A. E., Lauvaux, T., West, T. O., Denning, A. S., Davis, K. J., Miles, N., Richardson, S., Uliasz, M., Lokupitiya, E., Cooley, D., Andrews, A., and Ogle, S.: Evaluating atmospheric CO_2 inversions at multiple scales over a highly inventoried agricultural landscape, Global Change Biology, 19, 1424–1439, https://doi.org/10.1111/gcb.12141, 2013.

Schuur, E. A. G., Bracho, R., Celis, G., Belshe, E. F., Ebert, C., Ledman, J., Mauritz, M., Pegoraro, E. F., Plaza, C., Rodenhizer, H., Romanovsky, V., Schädel, C., Schirokauer, D., Taylor, M., Vogel, J. G., and Webb, E. E.: Tundra Underlain

By Thawing Permafrost Persistently Emits Carbon to the Atmosphere Over 15 Years of Measurements, Journal of Geophysical Research: Biogeosciences, 126, e2020JG006044, https://doi.org/10.1029/2020JG006044, 2021.

Seddon, A. W. R., Macias-Fauria, M., Long, P. R., Benz, D., and Willis, K. J.: Sensitivity of global terrestrial ecosystems to climate variability, Nature, 531, 229–232, https://doi.org/10.1038/nature16986, 2016.

Shen, W., Jenerette, G. D., Hui, D., and Scott, R. L.: Precipitation legacy effects on dryland ecosystem carbon fluxes: direction, magnitude and biogeochemical carryovers, Biogeosciences, 13, 425–439, https://doi.org/10.5194/bg-13-425-2016, 2016.

Shiga, Y. P., Tadić, J. M., Qiu, X., Yadav, V., Andrews, A. E., Berry, J. A., and Michalak, A. M.: Atmospheric CO_2 Observations Reveal Strong Correlation Between Regional Net Biospheric Carbon Uptake and Solar-Induced Chlorophyll Fluorescence, Geophysical Research Letters, 45, 1122–1132, https://doi.org/10.1002/2017GL076630, 2018.

Stinson, G., Kurz, W. A., Smyth, C. E., Neilson, E. T., Dymond, C. C., Metsaranta, J. M., Boisvenue, C., Rampley, G. J., Li, Q., White, T. M., and Blain, D.: An inventory-based analysis of Canada's managed forest carbon dynamics, 1990 to 2008, Global Change Biology, 17, 2227–2244, https://doi.org/10.1111/j.1365-2486.2010.02369.x, 2011.

Swain, D. L., Tsiang, M., Haugen, M., Singh, D., and Diffenbaugh, N. S.: The extraordinary California drought of 2013/2014: Character, context, and the role of climate change, Bulletin of the American Meteorological Society, 95, S3–S7, 2014.

Tadono, T., Nagai, H., Ishida, H., Oda, F., Naito, S., Minakawa, K., and Iwamoto, H.: GENERATION OF THE 30 M-MESH GLOBAL DIGITAL SURFACE MODEL BY ALOS PRISM, The International Archives of the Photogrammetry, Remote Sensing and Spatial Information Sciences, XLI-B4, 157–162, https://doi.org/10.5194/isprs-archives-XLI-B4-157-2016, 2016.

Takaku, J., Tadono, T., Doutsu, M., Ohgushi, F., and Kai, H.: UPDATES OF 'AW3D30' ALOS GLOBAL DIGITAL SURFACE MODEL WITH OTHER OPEN ACCESS DATASETS, The International Archives of the Photogrammetry, Remote Sensing and Spatial Information Sciences, XLIII-B4-2020, 183–189, https://doi.org/10.5194/isprs-archives-XLIII-B4-2020-183-2020, 2020.

Tao, F., Chen, Y., and Fu, B.: Impacts of climate and vegetation leaf area index changes on global terrestrial water storage from 2002 to 2016, Science of The Total Environment, 724, 138298, https://doi.org/10.1016/j.scitotenv.2020.138298, 2020.

Venturini, A.: Climate change, risk factors and stock returns: A review of the literature, International Review of Financial Analysis, 79, 101934, https://doi.org/10.1016/j.irfa.2021.101934, 2022.

Vicca, S., Bahn, M., Estiarte, M., van Loon, E. E., Vargas, R., Alberti, G., Ambus, P., Arain, M. A., Beier, C., Bentley, L. P., Borken, W., Buchmann, N., Collins, S. L., de Dato, G., Dukes, J. S., Escolar, C., Fay, P., Guidolotti, G., Hanson, P. J., Kahmen, A., Kröel-Dulay, G., Ladreiter-Knauss, T., Larsen, K. S., Lellei-Kovacs, E., Lebrija-Trejos, E., Maestre, F. T., Marhan, S., Marshall, M., Meir, P., Miao, Y., Muhr, J., Niklaus, P. A., Ogaya, R., Peñuelas, J., Poll, C., Rustad, L. E., Savage, K., Schindlbacher, A., Schmidt, I. K., Smith, A. R., Sotta, E. D., Suseela, V., Tietema, A., van Gestel, N., van Straaten, O., Wan, S., Weber, U., and Janssens, I. A.: Can current moisture responses predict soil CO_2 efflux under altered

https://doi.org/10.5194/essd-2026-418
Preprint. Discussion started: 24 July 2026

precipitation regimes? A synthesis of manipulation experiments, Biogeosciences, 11, 2991–3013, https://doi.org/10.5194/bg-11-2991-2014, 2014.

Virkkala, A.-M., Aalto, J., Rogers, B. M., Tagesson, T., Treat, C. C., Natali, S. M., Watts, J. D., Potter, S., Lehtonen, A., Mauritz, M., Schuur, E. A. G., Kochendorfer, J., Zona, D., Oechel, W., Kobayashi, H., Humphreys, E., Goeckede, M., Iwata, H., Lafleur, P. M., Euskirchen, E. S., Bokhorst, S., Marushchak, M., Martikainen, P. J., Elberling, B., Voigt, C., Biasi, C., Sonnentag, O., Parmentier, F.-J. W., Ueyama, M., Celis, G., St.Louis, V. L., Emmerton, C. A., Peichl, M., Chi, J., Järveoja, J., Nilsson, M. B., Oberbauer, S. F., Torn, M. S., Park, S.-J., Dolman, H., Mammarella, I., Chae, N., Poyatos, R., López-Blanco, E., Christensen, T. R., Kwon, M. J., Sachs, T., Holl, D., and Luoto, M.: Statistical upscaling of ecosystem CO_2 fluxes across the terrestrial tundra and boreal domain: Regional patterns and uncertainties, Global Change Biology, 27, 4040–4059, https://doi.org/10.1111/gcb.15659, 2021.

Walker, A. P., De Kauwe, M. G., Bastos, A., Belmecheri, S., Georgiou, K., Keeling, R. F., McMahon, S. M., Medlyn, B. E., Moore, D. J. P., Norby, R. J., Zaehle, S., Anderson-Teixeira, K. J., Battipaglia, G., Brienen, R. J. W., Cabugao, K. G., Cailleret, M., Campbell, E., Canadell, J. G., Ciais, P., Craig, M. E., Ellsworth, D. S., Farquhar, G. D., Fatichi, S., Fisher, J. B., Frank, D. C., Graven, H., Gu, L., Haverd, V., Heilman, K., Heimann, M., Hungate, B. A., Iversen, C. M., Joos, F., Jiang, M., Keenan, T. F., Knauer, J., Körner, C., Leshyk, V. O., Leuzinger, S., Liu, Y., MacBean, N., Malhi, Y., McVicar, T. R., Penuelas, J., Pongratz, J., Powell, A. S., Riutta, T., Sabot, M. E. B., Schleucher, J., Sitch, S., Smith, W. K., Sulman, B., Taylor, B., Terrer, C., Torn, M. S., Treseder, K. K., Trugman, A. T., Trumbore, S. E., van Mantgem, P. J., Voelker, S. L., Whelan, M. E., and Zuidema, P. A.: Integrating the evidence for a terrestrial carbon sink caused by increasing atmospheric CO_2, New Phytologist, 229, 2413–2445, https://doi.org/10.1111/nph.16866, 2021.

Weiss, J. L., Overpeck, J. T., and Cole, J. E.: Warmer Led to Drier: Dissecting the 2011 Drought in the Southern U.S., 2012.

White, M. A., Thornton, P. E., Running, S. W., and Nemani, R. R.: Parameterization and Sensitivity Analysis of the BIOME–BGC Terrestrial Ecosystem Model: Net Primary Production Controls, Earth Interactions, 4, 1–85, https://doi.org/10.1175/1087-3562(2000)004%3C0003:PASAOT%3E2.0.CO;2, 2000.

Wofsy, S. C., Goulden, M. L., Munger, J. W., Fan, S.-M., Bakwin, P. S., Daube, B. C., Bassow, S. L., and Bazzaz, F. A.: Net Exchange of CO_2 in a Mid-Latitude Forest, Science, 260, 1314–1317, https://doi.org/10.1126/science.260.5112.1314, 1993.

Wu, D., Zhao, X., Liang, S., Zhou, T., Huang, K., Tang, B., and Zhao, W.: Time-lag effects of global vegetation responses to climate change, Global Change Biology, 21, 3520–3531, https://doi.org/10.1111/gcb.12945, 2015.

Xiao, J., Zhuang, Q., Baldocchi, D. D., Law, B. E., Richardson, A. D., Chen, J., Oren, R., Starr, G., Noormets, A., Ma, S., Verma, S. B., Wharton, S., Wofsy, S. C., Bolstad, P. V., Burns, S. P., Cook, D. R., Curtis, P. S., Drake, B. G., Falk, M., Fischer, M. L., Foster, D. R., Gu, L., Hadley, J. L., Hollinger, D. Y., Katul, G. G., Litvak, M., Martin, T. A., Matamala, R., McNulty, S., Meyers, T. P., Monson, R. K., Munger, J. W., Oechel, W. C., Paw U, K. T., Schmid, H. P., Scott, R. L., Sun, G., Suyker, A. E., and Torn, M. S.: Estimation of net ecosystem carbon exchange for the conterminous United States by combining MODIS and AmeriFlux data, Agricultural and Forest Meteorology, 148, 1827–1847, https://doi.org/10.1016/j.agrformet.2008.06.015, 2008.

Xiao, J., Zhuang, Q., Law, B. E., Baldocchi, D. D., Chen, J., Richardson, A. D., Melillo, J. M., Davis, K. J., Hollinger, D. Y., Wharton, S., Oren, R., Noormets, A., Fischer, M. L., Verma, S. B., Cook, D. R., Sun, G., McNulty, S., Wofsy, S. C., Bolstad, P. V., Burns, S. P., Curtis, P. S., Drake, B. G., Falk, M., Foster, D. R., Gu, L., Hadley, J. L., Katul, G. G., Litvak, M., Ma, S., Martin, T. A., Matamala, R., Meyers, T. P., Monson, R. K., Munger, J. W., Oechel, W. C., Paw, U. K. T., Schmid, H. P., Scott, R. L., Starr, G., Suyker, A. E., and Torn, M. S.: Assessing net ecosystem carbon exchange of U.S. terrestrial ecosystems by integrating eddy covariance flux measurements and satellite observations, Agricultural and Forest Meteorology, 151, 60–69, https://doi.org/10.1016/j.agrformet.2010.09.002, 2011.

Xiao, J., Ollinger, S. V., Frolking, S., Hurtt, G. C., Hollinger, D. Y., Davis, K. J., Pan, Y., Zhang, X., Deng, F., Chen, J., Baldocchi, D. D., Law, B. E., Arain, M. A., Desai, A. R., Richardson, A. D., Sun, G., Amiro, B., Margolis, H., Gu, L., Scott, R. L., Blanken, P. D., and Suyker, A. E.: Data-driven diagnostics of terrestrial carbon dynamics over North America, Agricultural and Forest Meteorology, 197, 142–157, https://doi.org/10.1016/j.agrformet.2014.06.013, 2014.

Xiong, C., Ma, H., Liang, S., He, T., Zhang, Y., Zhang, G., and Xu, J.: Improved global 250 m 8-day NDVI and EVI products from 2000–2021 using the LSTM model, Sci Data, 10, 800, https://doi.org/10.1038/s41597-023-02695-x, 2023.

Yadav, V. S., Yadav, S. S., Gupta, S. R., Meena, R. S., Lal, R., Sheoran, N. S., and Jhariya, M. K.: Carbon sequestration potential and CO_2 fluxes in a tropical forest ecosystem, Ecological Engineering, 176, 106541, https://doi.org/10.1016/j.ecoleng.2022.106541, 2022.

Yao, Y., Li, Z., Wang, T., Chen, A., Wang, X., Du, M., Jia, G., Li, Y., Li, H., Luo, W., Ma, Y., Tang, Y., Wang, H., Wu, Z., Yan, J., Zhang, X., Zhang, Y., Zhang, Y., Zhou, G., and Piao, S.: A new estimation of China's net ecosystem productivity based on eddy covariance measurements and a model tree ensemble approach, Agricultural and Forest Meteorology, 253–254, 84–93, https://doi.org/10.1016/j.agrformet.2018.02.007, 2018.

Yin, Y., Byrne, B., Liu, J., Wennberg, P. O., Davis, K. J., Magney, T., Köhler, P., He, L., Jeyaram, R., Humphrey, V., Gerken, T., Feng, S., Digangi, J. P., and Frankenberg, C.: Cropland Carbon Uptake Delayed and Reduced by 2019 Midwest Floods, AGU Advances, 1, e2019AV000140, https://doi.org/10.1029/2019AV000140, 2020.

Yu, G., Jia, Y., He, N., Zhu, J., Chen, Z., Wang, Q., Piao, S., Liu, X., He, H., Guo, X., Wen, Z., Li, P., Ding, G., and Goulding, K.: Stabilization of atmospheric nitrogen deposition in China over the past decade, Nat. Geosci., 12, 424–429, https://doi.org/10.1038/s41561-019-0352-4, 2019.

Zeng, J., Matsunaga, T., Tan, Z.-H., Saigusa, N., Shirai, T., Tang, Y., Peng, S., and Fukuda, Y.: Global terrestrial carbon fluxes of 1999–2019 estimated by upscaling eddy covariance data with a random forest, Sci Data, 7, 313, https://doi.org/10.1038/s41597-020-00653-5, 2020.

Zou, H., Chen, J., Li, X., Abraha, M., Zhao, X., and Tang, J.: Modeling net ecosystem exchange of CO_2 with gated recurrent unit neural networks, Agricultural and Forest Meteorology, 350, 109985, https://doi.org/10.1016/j.agrformet.2024.109985, 2024.